Analytical modeling of textile reinforced concrete (TRC) sandwich panels: Consideration of nonlinear behavior and failure modes

Zakaria Ilyes Djamai, Kamal Erroussafi, Amir Si Larbi, Ferdinando Salvatore, Gaochuang Cai

Analytical modeling of textile reinforced concrete (TRC) sandwich panels: Consideration of nonlinear behavior and failure modes

Zakaria Ilyes Djamai[a], Kamal Erroussafi[b,c], Amir Si Larbi[c], Ferdinando Salvatore[c], and Gaochuang Cai[c]

[a]LMDC (Laboratoire Matériaux et Durabilité des Constructions), Université de Toulouse, INSA/UPS Génie Civil, Toulouse, France; [b]EMI, Ecole Mohammadia d'Ingénieurs (LGC-BPC), Rabat Agdal, Maroc; [c]Université de Lyon, Ecole Nationale d'ingénieurs de Saint-Etienne (ENISE), Laboratoire de Tribologie et de Dynamique des Systémes (LTDS), Saint-Etienne, France

ABSTRACT

The emergence of new composite materials in the building industry allows textile reinforced con-crete (TRC) to be used in many industrial applications such as structural strengthening and new lightweight structures. One of the most promising applications of TRC is as a potential alternative to steel reinforced concrete and fiber reinforced polymer (FRP) used in the skins of foamed sand-wich panels. This study proposes an analytical method of designing TRC sandwich panels. Additionally, the method allows the load bearing capacity of TRC sandwich panels under bending solicitation to be calculated. The proposed model can promote TRC applications in the engineer-ing and building industry. The proposed model considers the nonlinear behavior of TRC using the ACK approach for evaluating the axial and bending stiffness of TRC in the multicracking and tex-tile transmission phases. Furthermore, the foam shear strains and foam hardening during bending solicitations are considered. The analytical approach was validated based on experimental data, and the validation process implemented was used to investigate the evolution of local strains in TRC skins to ensure the robustness of the developed model.

1. Introduction

Sandwich panels have widely emerged in the building industry because their concept combines the development of lightweight structures with high flexural stiffness and good thermal and acoustic insulation. Sandwich panels often consist of two rigid facings and a thicker cellular core. The skin faces usually consist of steel reinforced concrete; however the design codes require thick covers to prevent steel corrosion which constitutes a barrier to attaining lightweight sandwich panels. Some researchers [1, 2] have focused on the use of fiber reinforced polymer (FRP) as sandwich panel skins. However, FRP has the constraints in terms of cost and the criteria of sustainable development, in addition to poor thermal stability, flammability and the toxicity of the fumes released from the polymer.

Textile reinforced concrete (TRC) [3–5] consists of a fine-grained concrete matrix reinforced by a high-strength non-corroding textile made of alkali resistant glass, carbon etc …. .TRC exhibits high performance characteristics that combine the high compressive strength of plain concrete with the high tensile strength of textile fibers. Furthermore, TRC composites are considered a viable alternative to steel reinforced concrete and FRP in lightweight sandwich panels since they can ensure incombustibility and fire resistance that is attributed to their concrete matrix.

A growing sement of the scientific community is using TRCs in the manufacturing of sandwich panels. Shams et al. [5] investigated the performance of TRC sandwich panels reinforced with shear grid and metallic connectors in pure shear and bending solicitations. Junes [6] studied the load bearing capacity of a sandwich panel made of TRC skins reinforced with two layers of AR-glass MAT textile and a polyurethane foam core under a four-point bending test. Colombo [7] studied the effect of the panel scale on the failure mode of sandwich panels made with TRC skins and polystyrene foam core under bending tests. Vervloet et al. [8] studied the buckling behavior of Textile Reinforced Cement sandwich panels with varying face thickness using Digital Image.

Meanwhile, numerical models have been established to estimate the global behavior of TRC sandwich panels in terms of force versus deflection during bending tests. Cuypers [9] used the ANSYS program to model a TRC sandwich panel subjected to a four-point bending test using an experimental TRC macroscopic law of behavior. Djamai et al. [10] established a multiscale numerical model using the commercial program ABAQUS that integrates textile-concrete interaction laws to simulate the bending behavior of TRC sandwich panels. Portal et al. [11] studied the structural performance of an innovative TRC-Foam Concrete sandwich panel containing GFRP plate and pin connectors using both experimental tests (quasi static and cyclic) and the finite element method.

CONTACT Zakaria Ilyes Djamai djamai@insa-toulouse.fr LMDC (Laboratoire Matériaux et Durabilité des Constructions), Université de Toulouse, INSA/UPS Génie Civil, Toulouse, France.

The brief literature review above demonstrates that despite the good results achieved using numerical models for predicting the global behavior of TRC sandwich panels (in terms of force versus deflection), these models have limitations. They are time consuming especially when considering concrete multicracking and textile/concrete bond as in the case of TRC. They are sensible to the mesh without forgetting the complexity of the software programs that are not always free for use.

To ensure the possible integration of TRC in engineering applications such as sandwich panels, clear rules on structural codes considering nonlinear behavior must be set to avoid obtaining extreme factors of security.

Accordingly, this paper introduces a simplified analytical method that allows the evaluation of global load–deflection of TRC sandwich panels typically used as façade panels under bending solicitation.

The proposed analytical model is a further extension and developement of the work performed by [6, 12]. The purpose of the model is to estimate the load bearing capacity of a simply supported TRC sandwich panel under any bending solicitation and any possible mode of failure, including tensile and compression failure of the TRC skins and foam shear crushing.

The main contributions of the proposed model can be summarized as follows:

- The nonlinear behavior of TRC (concrete multicracking and textile load transmission tendency) is considered
- The nonuse of labourious iterations and investigations to determine the states of strain in the TRC skins cross sections and the use of the ACK approach [13] to consider the evolution of axial and bending stiffness of TRC skins when concrete multicracking and textile load transmission occur during bending.
- Consideration of foam angular deformation and possible foam hardening (nonlinear behavior) during load computation.
- The model does not require any use of numerical techniques for resolution and computation.

Finally, the model aims to be presented as an engineer dimensioning tool for TRC sandwich panel applications. The validation of the proposed model is achieved through a comparison with the experimental result of a TRC sandwich panel realized in the laboratory.

2. Presentation of the analytical model

2.1. Hypothesis

The main constitutive hypothesis for developing the analytical model for TRC sandwich panels under uniaxial bending solicitation is derived from the sandwich panel theory developed by Allen [14] and improved by Stamm and Witte [15] for sandwich panels with rigid facing and soft core. The original theory [14, 15] is adapted to TRC sandwich panels; thus, the developed model assumes that:

- The TRC sandwich panel is considered a simply supported 1D compound beam.
- The hypothesis of small deformation is considered (strains are assumed to remain at a sufficiently low level)
- The cross section of the TRC sandwich panels does not remain plane due to shear deformation of the cellular core (Figure 1). Therefore, the Navier-Bernoulli hypothesis cannot be considered.
- While TRC skins have a much higher extensional stiffness than the core, normal stress does not occur in the core, and shear stress is assumed to be constant over the foam core height.
- The sandwich panel deformation consists of a foam shear angular strain and a beam bending deflection, and their effects are analyzed independently of each other.
- The nonlinear behavior of TRC (due to concrete multicracking and textile transmission tendency) and possible foam hardening are considered in the model.
- TRC skins can have significant bending stiffness around their own axis which must be taken into account. In fact, for the faces and core to remain in contact during bending of the sandwich panel, the faces must bend to an infinite curvature due to foam shear strain, which is physically impossible. Instead, the skins bend locally around their own axes (Figure 1). As a result, the locally created bending stresses must be considered, especially when concrete multicracking and concrete/textile load transfers are considered, such as the case of TRC.

2.2. Analytical development (original model developed in [15])

The governing equations of the bending behavior of a sandwich panel can be given as: (Figure 1)

$$M_s = B_s(\dot{\Upsilon} - w^{II}) = B_s \Upsilon_2 \tag{1}$$

$$M_u = -B_u w^{II} \tag{2}$$

$$M_l = -B_l w^{II} \tag{3}$$

$$Q_s = A\ \Upsilon \tag{4}$$

$$Q_u = -B_u w^{III} \tag{5}$$

$$Q_l = -B_l w^{III} \tag{6}$$

$$B = B_s + B_l + B_u \tag{7}$$

$$Q = Q_s + Q_l + Q_u \tag{8}$$

$$M = M_S + M_l + M_u \tag{9}$$

$$B_s = \frac{(EA)_l (EA)_u c^2}{(EA)_l + (EA)_u}$$

Indexes l, u refers to the lower and upper TRC skins and s refers to the sandwich part of the cross section.

M, Q, B are the total bending moment, shear force and bending stiffness in the sandwich panel, respectively.

M_s, M_u, M_l are the bending moment of the sandwich part of the cross section, and bending moment of the upper and lower TRC skins on their own axis, respectively.

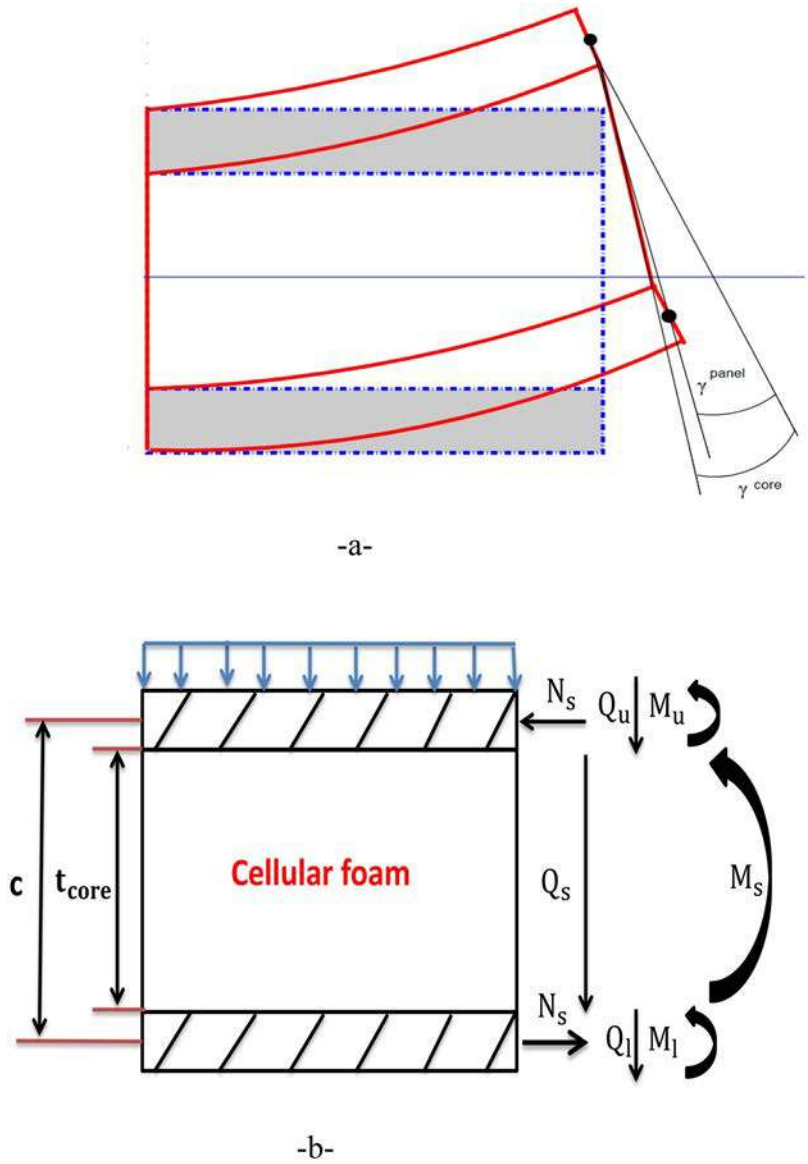

Figure 1. (a) Angular strains and (b) bending moments and shear forces on a sandwich panel under bending.

Q_s, Q_u, Q_l are the shear force in the sandwich part of the cross section and shear forces in the upper and lower TRC skins, respectively.

B_s, B_u, B_l are the bending stiffness of the sandwich part of the cross section, and bending stiffness of the upper and lower TRC skins on their own axis, respectively.

$(EA)_l$, $(EA)_u$ are the extensional stiffness of the lower and upper TRC skins, respectively.

Υ, w are the foam shear strain and panel bending deflection, respectively.

$A = Gb_p \frac{c^2}{t_{core}}$ is the panel shear stiffness.

G is the nominal shear modulus of the foam, t_{core} is the foam thickness and **c** is the distance between the inertial centers of the two TRC skins, b_p is the panel width.

For an arbitrary transverse loading -q(x), after eliminating w and Υ from Eqs. (8) and (9), respectively, the universal decoupled differential Eqs. (10) and (11) are:

$$-\frac{(B_u + B_l)}{A} w^{VI} + \frac{B}{B_s} w^{IV} = \frac{q}{B_s} - \frac{q^{II}}{A} \tag{10}$$

$$-\frac{(B_u + B_l)}{A} \Upsilon^{IV} + \frac{B}{B_s} \Upsilon^{II} = -\frac{q^{I}}{A} \tag{11}$$

Stamm and Witte [15] offered a system solution for a simply supported beam subjected to uniformly distributed load and a point load. The solution for a point load solicitation at any position x is given in [15] and in Appendix at the end of the manuscript.

2.3. Development of the new TRC sandwich panel analytical model

The solution proposed by [15] is valid for a sandwich beam with constant axial $[(EA)_l, (EA)_u]$ and bending (B_l, B_u) skins stiffness. However, when concrete multicracking occurs and force is transmitted from the cracked concrete to the textile, TRC skins bending and axial stiffness change during bending.

To consider the evolution of the TRC bending and axial stiffness in the new TRC sandwich panel analytical model, a

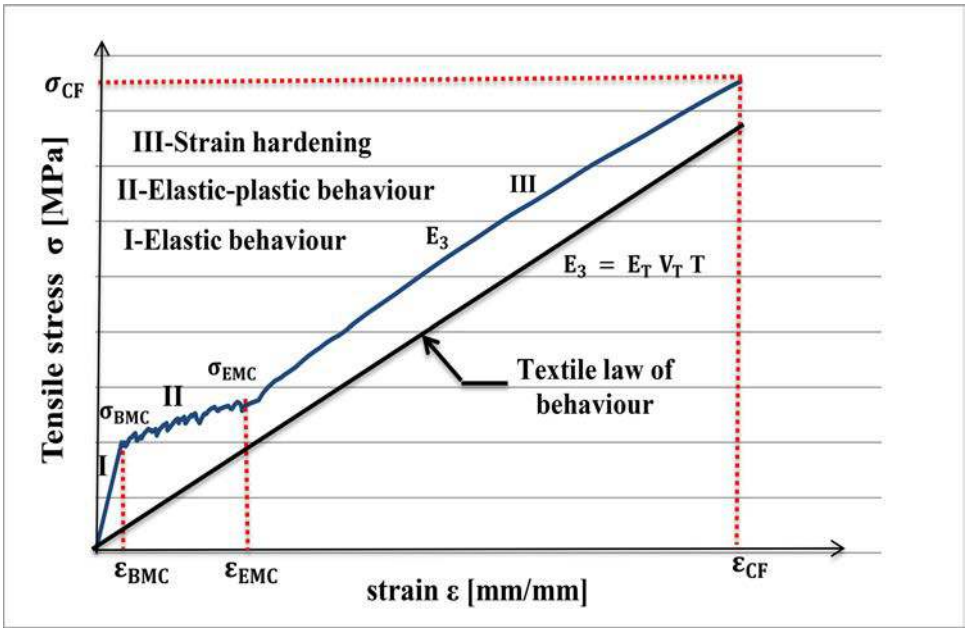

Figure 2. TRC stress-strain (σ-ε) behavior under direct tensile loading.

simplified method is proposed here based on the TRC characteristic constitutive laws (σ–ε) under uniaxial tensile and compression solicitations.

2.3.1. TRC constitutive laws

Under tensile solicitation, many authors [16] consider TRC to have a macroscopic tri-linear stress-strain relation (Figure 2).

In the first stage (**I**, Figure 2), TRC usually shows an elastic linear increase with a Young's modulus E_C corresponding to the matrix modulus. In the next stage, the concrete elastic yield stress σ_{BMC} is reached and cracks appear randomly in the matrix that transmits stress to the textile, which retransmits it back to the matrix until its elastic limit is reached again at another location. This repeated process creates a multicracking step (**II**, Figure 2). At the end, in the stage (**III**, Figure 2) the stress is transmitted almost entirely to the fabric, with final phase secant stiffness (E_3) corresponding to the textile stiffness.

ε_{BMC} and ε_{EMC} are the strains of the composite TRC at the beginning and the end of multicracking step, respectively.

σ_{CF}, ε_{CF} are the stress and strain of the composite at failure, respectively.

Under compression solicitation, although concrete can present nonlinear behavior at high strains (much higher than concrete tensile cracking strains), TRC behavior is assumed to be linear and almost-elastic until brutal failure due to interlaminar (textile/concrete) shear failure. This assumption is based on many experimental investigations [17].

2.3.1.1. Extraction of TRC axial stiffness under direct tensile solicitation. The axial secant stiffness of the TRCs skins evolves during bending of the sandwich panel according to the state of tensile strains on the cross section (Figure 2)

$$EA_{u,l} = E_C\ A_{u,l} \quad \text{for } 0 \le \varepsilon \le \varepsilon_{BMC}$$

$$EA_{u,l} = (EA)_{multicrack} \quad \text{for } \varepsilon_{BMC} \le \varepsilon \le \varepsilon_{EMC}$$

$$EA_{u,l} = E_T V_T\ T\ A_{u,l} \quad \text{for } \varepsilon_{EMC} \le \varepsilon \le \varepsilon_{CF}$$

where E_C is the concrete elastic Young's modulus. $A_{u,l}$ is the cross section of the upper, lower TRC facing and $(EA)_{multicrack}$ is the axial stiffness of TRC during multicracking (**deduced from stage II**, Figure 2).

E_T, V_T and T are the Young's modulus of the textile used, the volumetric rate of the textile reinforcement and the stiffness efficiency ratio, respectively ($T = \frac{E_3}{E_T V_T}$, E_3 is the stiffness of the composite TRC in the **stage III**, Figure 2).

Remark: the establishment of TRC axial stiffness during nonlinear behavior, allows an evaluation of the strain due the sandwich part of the sandwich moment M_s in TRC skins while bending of the sandwich panel (see further in Section 2.3.3.1).

2.3.1.2. Extraction of TRC bending stiffness during bending around its own axis (evolution of TRC moment versus curvature law of behavior during bending around its own axis due to $M_{u,l}$). Engineer designers can easily determine the TRC law of behavior and thus the evolution of axial stiffness under direct tensile solicitation (considering the simplicity of the experimental test). However, bending stiffness of TRC skins of the sandwich panel evolves as well while concrete multicracking and textile force transmission occur under bending and should be considered when developing the analytical model for TRC sandwich panel.

The main hypothesis used to determine the TRC moment–curvature law of behavior and the evolution of TRC skin bending stiffness includes the following:

- The TRC laws of behavior described in Section 2.3.1 allow for the TRC strain and stress evolution in the cross section during bending to be evaluated.

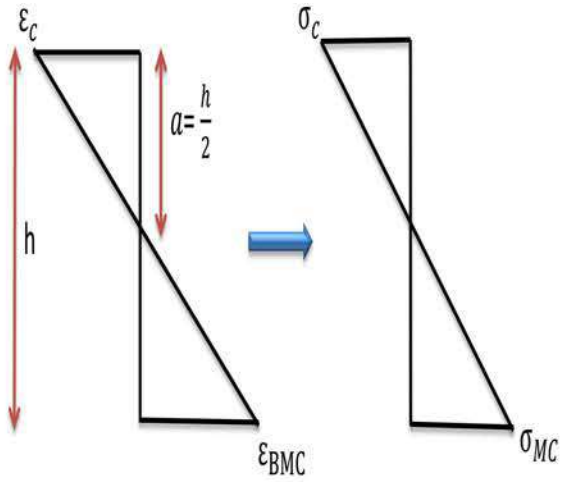

-a-

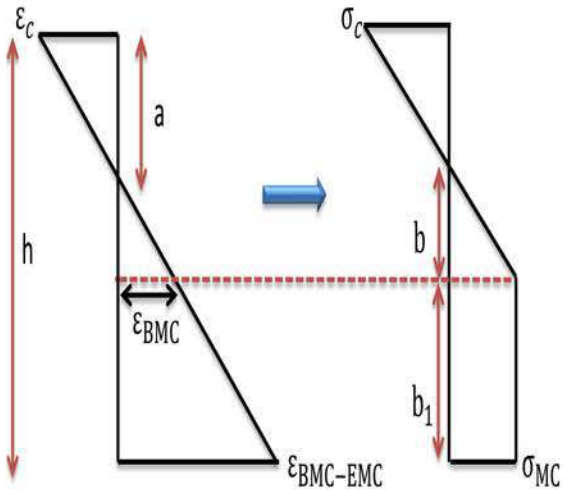

-b-

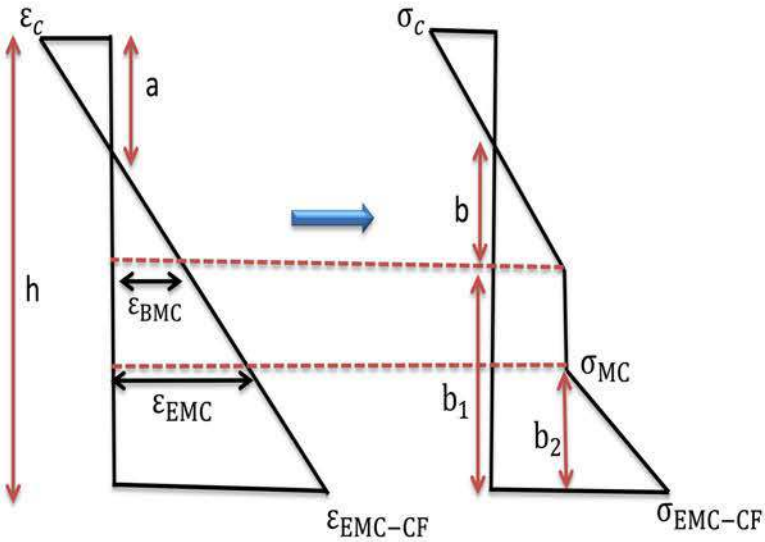

-c-

Figure 3. Stress and strain distribution in TRC cross section during bending in (a) elastic, (b) multi-cracking and (c) textile transmission phase.

- Linear distribution of normal strains due to bending of TRC facing on their own axis (TRC cross section remains plane during bending on its own axis).
- Strains remain at a sufficiently low level (hypothesis of small deformations).
- The position of the neutral axis evolves in TRC skin cross section during concrete multicraking and concrete/ textile stress transmission under bending.

The developed procedure uses the ACK approach [13] to evaluate the bending stiffness of TRC skins, while the states of stress and strain evolve during bending around their own axis (in the three characteristics phases, Figure 2).

2.3.1.2.1. Elastic phase (I, Figure 2). At the end of the elastic phase, the states of strain and stress in the TRC cross section during bending can be shown as Figure 3a:

ε_C is the strain of the extreme compressed facing
a is the distance of the neutral axis from the extreme compressed facing.
h is the thickness of the TRC cross section.

In the elastic phase $a = \frac{h}{2}$.

- The equilibrium of forces at the end of the elastic phase leads to:

$$\frac{1}{2}\ E_C\ \varepsilon_C\ \ a = \frac{1}{2}\ E_C\ \varepsilon_{BMC}\ a \tag{12}$$

- Moment equilibrium leads to

$$M = \frac{1}{3}\ E_C\ \varepsilon_{BMC}\ a^2\ \ + \frac{1}{3}\ E_C\ \varepsilon_C\ a^2 = \frac{2}{3}\ E_C\ \varepsilon_{BMC}\ a^2 \tag{13}$$

At this moment, the curvature $\theta = \frac{\varepsilon_C + \varepsilon_{BMC}}{h}$, $B_{u,1\ elas} = \frac{M}{\theta}$
$B_{u,1\ elas}$ is the TRC skin secant bending stiffness during the elastic phase.

2.3.1.2.2. Multicracking phase (II, Figure 2). In the multicracking phase, the state of strain and stress in the TRC cross section during bending can be shown as Figure 3b.

For analytical purposes, an idealistic stress-strain relation is considered, which is based on the assumption that the multicracking phase occurs at an almost constant stress (σ_{MC}). This hypothesis has been assumed for the ACK model presented in [13].

The symbol $\varepsilon_{BMC-EMC}$ (Figure 3b) is assigned for the strain of the extreme tensioned face of TRC where strain extends from ε_{BMC} to ε_{EMC}.

σ_{MC} is the constant stress corresponding to the concrete multi-cracking step (**stage II,** Figure 2), which is assumed to be the mean value of (σ_{BMC} and σ_{EMC}).

The equations of geometrical compatibility lead to:

$$\frac{\varepsilon_c}{a} = \frac{\varepsilon_{BMC-EMC}}{h-a} \tag{14}$$

$$\frac{\varepsilon_{BMC}}{b} = \frac{\varepsilon_c}{a} \tag{15}$$

$$b + b_1 + a = h \tag{16}$$

The equilibrium of forces on the stress diagram yields:

$$E_C\ \varepsilon_{BMC-EMC}\ \frac{a^2}{2\ (h-a)} = b\ \frac{\sigma_{MC}}{2}\ + b_1\sigma_{MC} \tag{17}$$

The equilibrium of the moments on the neutral axis yields:

$$E_C\ \varepsilon_{BMC-EMC}\frac{a^3}{3(h-a)} + b^2\frac{\sigma_{mc}}{3} + \sigma_{MC}b_1\left(\frac{b_1}{2}+b\right) = M \tag{18}$$

The solution of the system of five Eqs. (14), (15), (16), (17), (18) leads to the evaluation of the unknown variables ε_c, a, b, b_1 and M for a given (predefined) value of $\varepsilon_{BMC-EMC}$.

At this moment, the curvature in the multi-cracking step is

$$\theta = \frac{\varepsilon_{BMC-EMC} + \varepsilon_C}{h}\ \ B_{u,1\ multicrak} = \frac{M}{\theta}$$

$B_{u,1\ multicrak}$ is the TRC skin tangential bending stiffness during the multicracking step.

2.3.1.2.3. Textile transmission phase (III, Figure 2). The symbols ε_{EMC-CF}, σ_{EMC-CF} (Figure 3c) are assigned for strain and stress of the extreme tensioned face of TRC, respectively, where strain extends from ε_{EMC} to ε_{CF} and stress extends from σ_{MC} to σ_{CF}.

The equations of geometrical compatibility lead to:

$$\frac{\varepsilon_{BMC}}{b} = \frac{\varepsilon_c}{a} \tag{19}$$

$$\frac{\varepsilon_{EMC-CF}}{h-a} = \frac{\varepsilon_c}{a} \tag{20}$$

$$\frac{\varepsilon_c}{a} = \frac{\varepsilon_{EMC}}{h-a-b_2} \tag{21}$$

$$b + b_1 + a = h \tag{22}$$

The equilibrium of forces on the stress diagram yields:

$$E_C\ \varepsilon_{EMC-CF}\ \frac{a^2}{2\ (h-a)} = b\frac{\sigma_{MC}}{2} + b_1\sigma_{MC} + E_T V_T\ T\ (\varepsilon_{EMC-CF} - \varepsilon_{EMC})\frac{b_2}{2} \tag{23}$$

The equilibrium of the moments on the neutral axis yields:

$$E_C\ \varepsilon_{EMC-CF}\frac{a^3}{3(h-a)} + b^2\frac{\sigma_{MC}}{3} + \sigma_{MC}b_1\left(\frac{b_1}{2}+b\right) + E_T V_T\ T\ \left(h-a-\frac{b_2}{3}\right)(\varepsilon_{EMC-CF} - \varepsilon_{EMC})\frac{b_2}{2} = M \tag{24}$$

The solution of the system of six Eqs. (19), (20), (21), (22), (23), (24) leads to the evaluation of the unknown variables ε_c, a, b, b_1, b_2, and M for a given (predefined) value of ε_{EMC-CF}.

$$\theta = \frac{\varepsilon_{EMC-CF} + \varepsilon_C}{h}\ \text{ and }\ B_{u,1\ textrans} = \frac{M}{\theta}$$

$B_{u,1\ textrans}$ is the TRC skin secant bending stiffness during the textile transmission step.

Remark: the establishment of TRC bending stiffness in the phases (I,II,III) allows an evaluation of the strain due to bending of TRC skin around its own axis (attributed to $M_{u,1}$) while bending of the sandwich panel (see further Section 2.3.3.1).

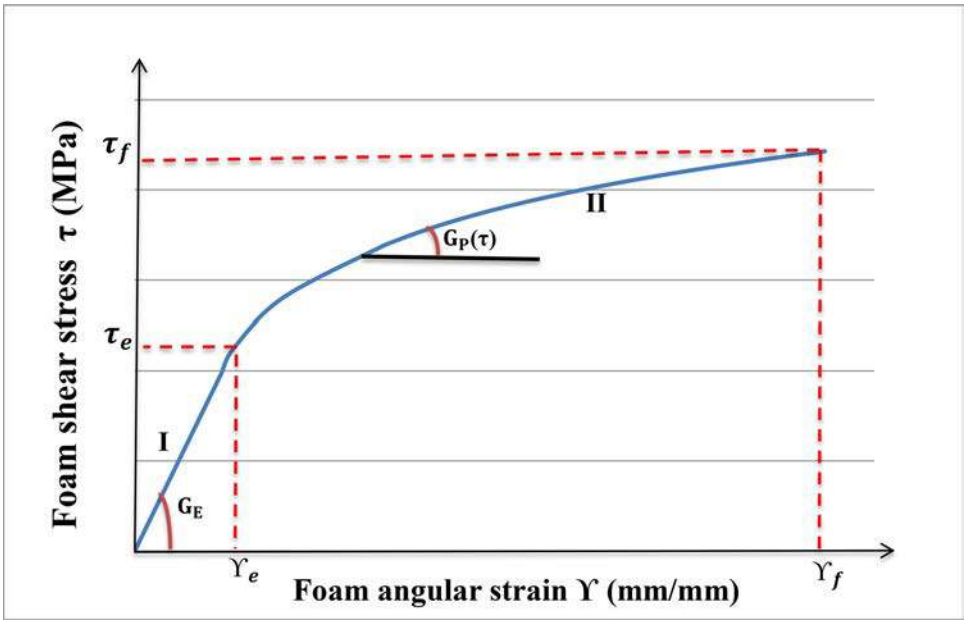

Figure 4. Cellular foam law of behavior under pure shear loading.

2.3.2. Foam constitutive law of behavior

The response of cellular foam under pure shear is presented (Figure 4). In the first phase (**I**, Figure 4), the response of the foam is elastic with a secant shear modulus G_e. After reaching the shear yield stress τ_e; the response is nonlinear (foam hardening phase), it is characterized by bending of the foam cell walls until the ultimate strain at failure Υ_f is reached (**II**, Figure 4). The foam tangential shear stiffness at this moment depends on the state of shear stress $G_p(\tau)$ [18].

Remark: It should be emphasized for the reader that the authors speak about the secant axial stiffness for TRC (tri-linear law of behavior) when they speak about the tangential shear stiffness in the case of the core during foam hardening.

2.3.3. Implementation of the new analytical model

2.3.3.1. Main assumptions for computation. The main theory of the proposed new sandwich panel model derives from the model proposed by Stamm and Witte [15] that extends (by considering the own bending stiffness of the skins) the classical assumptions elaborated in the books of Allen and Plantema [14]. This model has already been used in the context of TRC by Shams [12] who include the nonlinear behavior of the skins. The new proposed analytical model uses in this regard the ACK approach for the TRC tensile behavior, by which it distinguishes itself from the approach of [12].

The consideration of the ACK approach allows for a quick computation of the states of stress and strain in TRC skins and an easy evaluation of the evolution of their bending stiffness during nonlinear behavior which must be considered, especially in the case of thick skins.

The new analytical model is implemented following the subsequent steps:

- The hypothesis of simply supported panel subjected to any load combination is adopted here.
- A quasi static loading is applied on the sandwich panel from $j = 0$ to $j = n$ increment of force.

The objective is to propose a simplified analytical approach for TRC sandwich panels that allows for predicting the behavior of the panel considering the nonlinear behavior of TRC (including concrete multicracking and textile transmission states) and the foam shear strains (including foam hardening) using the mathematical resolution proposed by Stamm and Witte [15] (Section 2.2).

However, the Stamm and Witte universal resolution [15] is only applicable in the elastic state and for skins with constant axial and bending stiffness and constant foam shear stiffness

Therefore, a homogenized bending and axial stiffness along the panel span is proposed for TRCs skins as they evolve to the multicracking and textile transmission states under bending.

A homogenized shear stiffness is also proposed for cellular foam when foam hardening occurs to facilitate the implementation of the analytical model.

To establish the homogenized TRC bending and axial stiffness and homogenized foam shear stiffness, the sandwich beam is subdivided into n parts along the span.

Every subdivision corresponds to a coordinate x_0, x_1, $\ldots x_i \ldots \ldots, x_n$.

The resulting moments/forces in the TRC skins at every increment of force j on the panel span and for every position x_i are composed of:

1-A pure bending moment of TRC skins on their own axis due to $M_l(x_i)_j$ and $M_u(x_i)_j$ (see Figure 1), calculated at every position x_i according to Stamm and Witte solution [15] (see Appendix in the end of the manuscript).

The total bending moment of the skins on their own axis is $M_D(x_i)_j = M_l(x_i)_j + M_u(x_i)_j$ which is distributed according to the TRC skins bending stiffness. The resulting state of strain and stress (due to bending of TRC around their own

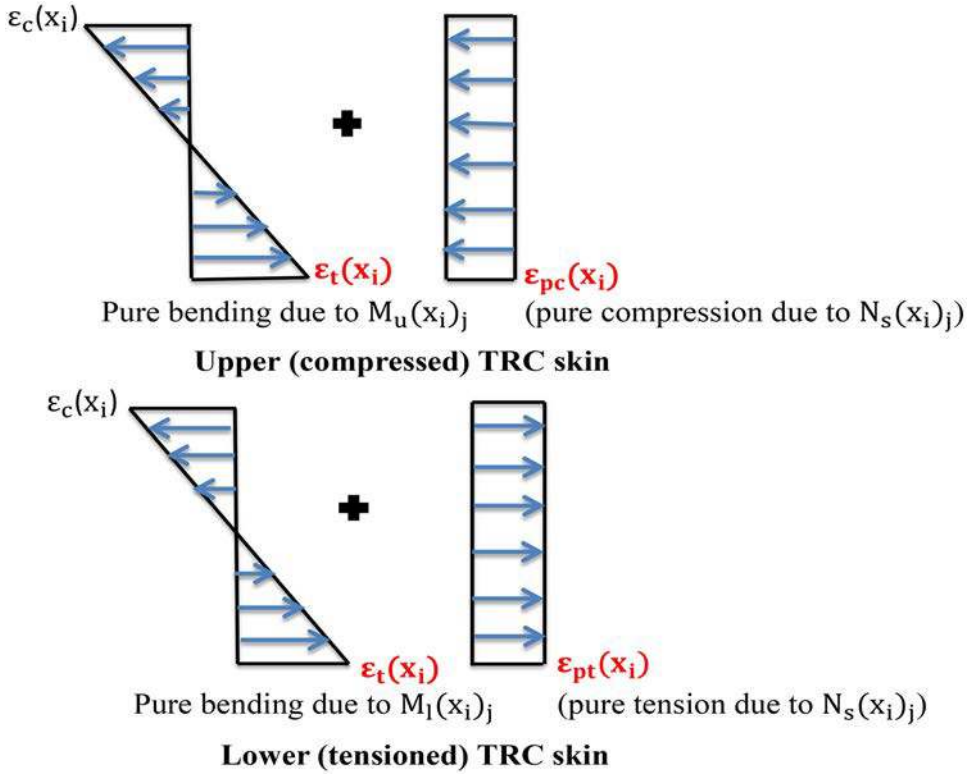

Figure 5. Distribution of strains in the textile reinforcement of TRC cross sections due to sandwich panel bending.

axis) is deduced from the procedure explained in Section 2.3.1.2 (see Section 2.3.1.2, extracting the state of stress and strain in TRC skins cross section due to bending around their own axes for a given moment $\mathbf{M_{u,l}}$ even during nonlinear behavior, the procedure described Section 2.3.1.2 also allows the evaluation of TRC bending stiffness during its nonlinear behavior).

2-A pure tensile force in the lower (tensioned) TRC skin as a result of the sandwich part of the moment $N_{s,l}(x_i)_j = \frac{M_s(x_i)_j}{c}$ (see Figure 1) [c is the distance between the inertial centers of the two TRC skins]. The resulting strain $\varepsilon_{pt}(x_i)_j$ (due to pure tensile loading) is deduced from the characteristic diagram (σ-ε) of TRC under pure tensile solicitation (see Section 2.3.1.1 and Figure 2 where the establishment of the axial stiffness of TRC during its nonlinear behavior allows the evaluation of $\boldsymbol{\varepsilon_{pt}(x_i)_j}$)

3-A pure compression force in the upper (compressed) TRC skin as a result of the sandwich part of the moment $N_{s,u}(x_i)_j = -N_{s,l}(x_i)_j$. The resulting strain $\varepsilon_{pc}(x_i)_j$ (due to the pure compression loading) is deduced from the characteristic diagram (σ-ε) of TRC under compression solicitation (elastic behavior of TRC under compression solicitation).

2.3.3.2. Strain superposition on the textile reinforcement. The principle of strain superposition cannot be applied to the concrete component of TRC skins as they evolve to the cracked state. However the textile reinforcement of the skins remains elastic and linear until failure of TRC under tensile solicitation due to the textile elastic brittle behavior (the law of behavior of the textile reinforcement with the law of behavior of TRC under direct tensile solicitation in the same graphic is presented Figure 2).

As a consequence, the final state of strain in the skin textile reinforcement is

A- For the upper (compressed) TRC skin

- The sum of the strain induced by pure bending of TRC on its own axis (attributed to $M_u(x_i)_j$) and the strain attributed to pure compression due to $M_s(x_i)_j$ (see Figure 5).

B- For the lower (tensioned) TRC skin

- The sum of the strain induced by pure bending of TRC on its own axis (attributed to $M_l(x_i)_j$) and the strain attributed to pure tension due to $M_s(x_i)_j$ (see Figure 5).

This implies:

The maximum strain in the extreme textile reinforcement fiber $\varepsilon_u(x_i)_{j_{max}}$ of the upper (compressed) TRC skin is $\varepsilon_t(x_i)_j - \varepsilon_{pc}(x_i)_j$.

The maximum strain in the extreme textile reinforcement fiber $\varepsilon_l(x_i)_{j_{max}}$ of the lower (tensioned) TRC skin is $\varepsilon_t(x_i)_j + \varepsilon_{pt}(x_i)_j$.where $\varepsilon_t(x_i)_j$ is the extreme positive strain (tension) due to bending of TRC skins on their own axis due to $M_u(x_i)_j$ or $M_l(x_i)_j$ (see Figure 5).

$\varepsilon_{pt}(x_i)_j$, $\varepsilon_{pc}(x_i)_j$ are the strains due to pure tension and pure compression, respectively induced by the sandwich part of the moment $N_s(x_i)_{u,l} = \pm \frac{M_s(x_i)_j}{c}$ (see Figure 5).

2.3.3.3. Homogenized TRC axial and bending stiffness. The evaluation of $\varepsilon_{u,l}(x_i)_{j_{max}}$ [$\varepsilon_l(x_i)_{j_{max}}$ for the tensioned TRC skin, $\varepsilon_u(x_i)_{j_{max}}$ for the compressed TRC skin] of the TRC

skin textile fabrics in the j increment of force allows the TRC skin bending and axial stiffness to be determined (actualized) at every position x_i ($\boldsymbol{\varepsilon_{u,1}(x_i)_{j_{max}}}$ is used as an indicator of the state of stiffness degradation) as follows:

$$\varepsilon_{u,1}(x_i)_{j_{max}} \leq 0 \text{ (compressed section)} \rightarrow (EA_{u,1}(x_i)_j = (E_C\ A_{u,1})_{elas},\ B_{u,1}(x_i)_{,j} = B_{u,l,elas})$$

$$\text{While } 0 \leq \varepsilon_{u,1}(x_i)_{j_{max}} \leq \varepsilon_{BMC} \rightarrow (EA_{u,1}(x_i)_j = (E_C\ A_{u,1})_{elas},\ B_{u,1}(x_i)_{,j} = B_{u,l,elas})$$

$$\varepsilon_{BMC} \leq \varepsilon_{u,1}(x_i)_{j_{max}} \leq \varepsilon_{EMC} \rightarrow (EA_{u,1}(x_i)_j = (EA)_{multicrack},\ B_{u,1}(x_i)_{,j} = B_{u,l,multicr})$$

$$\varepsilon_{EMC} < \varepsilon_{u,1}(x_i)_{j_{max}} \leq \varepsilon_{Cf} \rightarrow (EA_{u,1}(x_i)_j = E_T\ T\ V_T\ A_{u,1},\ B_{u,1}(x_i)_{,j} = B_{u,l,textrans})$$

$B_{u,l,elas}$, $B_{u,l,multicr}$ and $B_{u,l,textrans}$ are the bending stiffness of TRC skins during bending around its own axis (in the three characteristic stages of TRC behavior under tensile loading) evaluated according to the procedure described Section 2.3.1.2.

The actualization of the local stiffness $(EA_{u,1}(x_i)_j$, $B_{u,1}(x_i)_j)$ in the j increment of force at each position x_i allows the sandwich panel homogenized skin stiffness in the $j+1$ increment of force to be reevaluated. The homogenized skins bending and axial stiffness ($EA_{u,1\ homo,j+1}$, $B_{u,1\ homo,j+1}$) in the $j+1$ increment of force can be estimated by weighting the local stiffness of the skins $(EA_{u,1}(x_i)_j$, $B_{u,1}(x_i)_j)$ at every position x_i in the j increment of force by the corresponding maximum strains $\varepsilon_{u,1}(x_i)_{j_{max}}$(Eqs. 25 and 26)

$$EA_{u,1\ homo,j+1} = \frac{\sum_{i=0}^{i=n} EA_{u,1}(x_i)_j \times \varepsilon_{u,1}(x_i)_{j_{max}}}{\sum_{i=0}^{i=n} \varepsilon_{u,1}(x_i)_{j_{max}}} \quad (25)$$

$$B_{u,1\ homo,j+1} = \frac{\sum_{i=0}^{i=n} B_{u,1}(x_i)_j \times \varepsilon_{u,1}(x_i)_{j_{max}}}{\sum_{i=0}^{i=n} \varepsilon_{u,1}(x_i)_{j_{max}}} \quad (26)$$

Weighting the local TRC skins stiffness $EA_{u,1}(x_i)_{,j}$, $B_{u,1}(x_i)_{,j}$ at every position x_i by the corresponding maximum strains $\varepsilon_{u,1}(x_i)_{j_{max}}$ allows either the stiffness degradation of TRC due to concrete cracking and textile force transmission or the degree of stiffness degradation to be considered.

2.3.3.4. Homogenized foam shear stiffness. The evaluation of foam shear strain $\Upsilon(x_i)_{,j}$ at every position x_i in the j increment of force according to Stamm and Witte solution [15], allows the actualization of local foam tangential shear stiffness at every position x_i according to (see Figure 4):

$$A(x_i)_{,j} = G_e b \frac{c^2}{t_{core}} \text{ for } 0 \leq \Upsilon(x_i)_{,j} \leq \Upsilon_f$$

$$A(x_i)_{,j} = G_P(\tau)\ b \frac{c^2}{t_{core}} \text{ for } \Upsilon_e \leq \Upsilon(x_i)_{,j} \leq \Upsilon_f$$

The homogenized foam shear stiffness of the sandwich panel in the $j+1$ increment of force can be estimated by weighting the foam local shear stiffness $A(x_i)_j$ at every position x_i in the j increment of force by the corresponding foam angular strain $\Upsilon(x_i)_j$ (Eq. 27)

$$A_{homo,j+1} = \frac{\sum_{i=0}^{i=n} A(x_i)_j\ \Upsilon(x_i)_j}{\sum_{i=0}^{i=n} \Upsilon(x_i)_j} \quad (27)$$

Thereby, weighting foam shear stiffness $A(x_i)_j$ by the corresponding shear strain $\Upsilon(x_i)_j$ at every position x_i allows either the degradation of the foam stiffness due to shear or its degree of degradation to be considered.

The reevaluated homogenized stiffness ($EA_{u,1\ homo,j+1}$, $B_{u,1\ homo,j+1}$, $A_{,homo,j+1}$) in the $j+1$ increment of force are reintroduced in the universal Eqs. (10) and (11) for the reevaluation of the states of strain in the TRC skins and foam core at every position x_i until failure.

2.3.3.5. Failure modes (calculation stop criterion). The method discussed above allows the global behavior of a simply supported TRC sandwich panel subjected to bending to be determined and the state of strain at any arbitrary section in every increment of force j to be established. However, to end the incrementation process, a clear indicator of panel failure should be defined. The failure modes that introduce the failure criteria are as follows:

A -Tensile failure of TRC skin

- This mode occurs when the textile fabric tensile strain exceeds the strain at failure $\varepsilon_{u,1}(x_i)_{j_{max}} \geq \varepsilon_{cf}$

B-Compression crushing of TRC skin

- This mode occurs when the TRC compression stress exceeds the stress at failure $\sigma_{u,1}(x_i)_{j_{max}} \geq \sigma_{comp}$ where σ_{comp} is the compression strength of the TRC skin.

C-Foam shear failure

- This mode occurs when the shear plastic strain of the foam exceeds the shear strain at failure $\Upsilon(x_i)_j \geq \Upsilon_f$

2.3.3.6. Calculation flow chart. The global flow chart algorithm of the proposed model is summarized Figure 6.

3. Model validation

3.1. Model validation on sandwich panel with significant TRC bending stiffness

3.1.1. Description of the four-point bending test

The performance of the proposed analytical model was validated using an experimental four-point bending test conducted by the authors.

The test panel (1200 mm long× 86 mm thick × 300 mm wide) consisted of two TRC skins (12 mm thick for the upper (compressed skin), 28 mm thick for the lower (tensioned skin), see Figure 7(a and b) and an insulation layer made of polyurethane PU (46 mm thick).

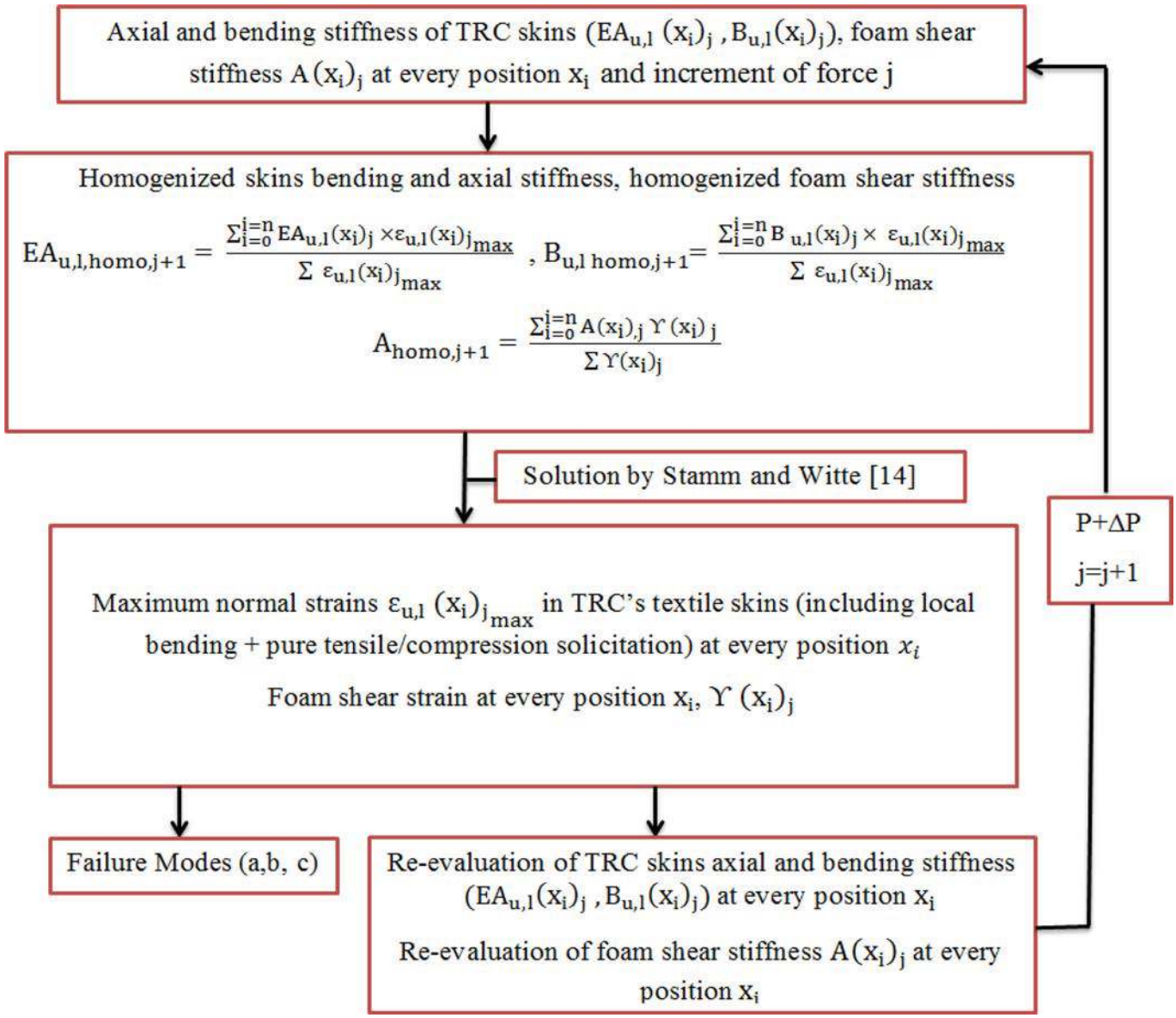

Figure 6. Analytical model: calculation chart.

- The thickness of the TRC skin under tension (28 mm) was chosen so as not to neglect the bending stiffness of the TRC facing on its own axis.
- The TRC skins consist of a fine-grained concrete (Young's modulus equal to 10 GPa) reinforced with a textile volumetric rate of reinforcement of 5.2% of latex coated alkali resistant glass fabric (corresponding to 3 layers of textile fabric in the upper and 7 layers in the lower TRC facing).
- The TRC skin law of behavior under quasi-static tensile loading was evaluated by an experimental tensile test realized according to the recommendation of the Rilem [19] on ($8 \times 70 \times 500$ mm) TRC specimens reinforced with the same textile volumetric rate of reinforcement of the TRC skins. The moment curvature law of behavior of TRC skins has been analytically evaluated using the procedure described (Section 2.3.1.2) with the TRC skin law of behavior under tensile loading as an input parameter.
- The characteristic parameters of TRC and foam laws of behavior under tensile and shear solicitation, respectively are summarized in Table 1 (The laws are also provided in the graphic form in Figure 8).
- The sandwich panel was tested in four-point bending in a displacement imposed (0.2mm/min) with a panel span of 1100 mm (distance of 366 mm between the loading knives and the supports).
- An LVDT sensor was used to measure the sandwich deflection at mid span. Two LVDT sensors placed at mid span and covering a measurement length of 200 mm were used to quantify the strains in the tensioned (lower) TRC skin (Figure 7).

3.1.2. Analytical model vs experimental results

3.1.2.1. Global behavior. The new analytical model for TRC sandwich panels and the experimental results are compared

-a-

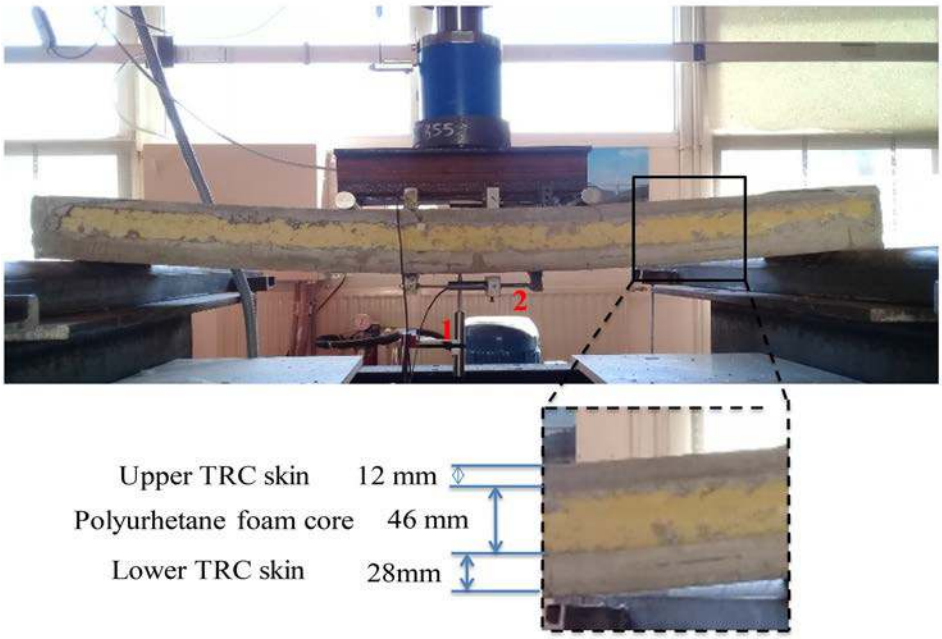

-b-

Figure 7. (a) Casting of TRC sandwich panels (b) Experimental four points bending test on TRC sandwich panel.

in terms of force transmitted vs deflection at mid span until failure; the two curves are plotted in Figure 9. A third curve in Figure 9 shows the analytical prediction of the sandwich panel mechanical behavior by considering the TRC skins bending stiffness on their own axis constant and equal to their elastic bending stiffness (neglecting the evolution of TRC skins bending stiffness) during the loading.

The theoretical model that considers the evolution of TRC axial and bending stiffness (**red squares**, Figure 9) and experimental investigation are consistent.

The behavior of the panel is divided into three stages.

[0 to ≈ 2900 N]: The behavior of the panel is governed by the elastic behavior of its components (TRC skins and foam core).

[2900 to 7300 N]: The first crack occurs at 2900 N in the lower TRC skin. This explains the slight decrease of the force transmitted. Increasing the applied force, the tensile yield is reached in the lower TRC skin and the concrete retransmits the stress back to the textile which retransmits the stress back to the matrix until the elastic limit is reached again at another location. At crack stabilization, the load in the lower TRC facing is almost entirely transferred to the textile reinforcement and the sandwich panel stiffness is governed by the lower TRC skin homogenized axial and bending stiffness which are approximately $[(EA)_l = E_T V_T T\ A_{u,l},\ B_l = B_{Textran}]$. The sandwich panel stiffness during TRC nonlinear behavior is well predicted by the analytical model that considers the TRC axial and bending stiffness evolution during bending. The sandwich panel stiffness is widely overestimated by the analytical model that only considers the evolution of TRC axial stiffness (the reasons will be detailed below).

[7300N to failure]: The panel stiffness decreases due to foam hardening which is well predicted by the analytical model that considers the two evolutions of TRC axial and bending stiffness. However, there is a slight difference between the model and the experiment that can be explained by the difficulty of accurately estimating the homogenized foam shear stiffness after hardening. The foam shear failure is also predicted by the analytical model (with an error of 7% in the applied force at failure between the analytical model and experiment).In comparison, the analytical model that only considers the evolution of TRC axial stiffness during bending, is unable to detect either foam hardening or shear failure.

Table 1. TRC and foam mechanical parameters used for model computation.

Characteristic parameters of TRC tensile stress vs strain law of behavior						
E_E [GPA]	ε_{BMC}	ε_{EMC}	ε_{CF}	σ_{BMC} [MPa]	σ_{EMC} [MPa]	σ_{CF} [MPa]
10	2.17×10^{-4}	2.2×10^{-3}	4.8×10^{-2}	2.05	2.68	10.5
TRC tensioned skin axial stiffness evolution during quasi static monotonic tensile test						
$(E_C\ A_{u,l})_{elas}$ [N]		$(E_C\ A_{u,l})_{multicrack}$ [N]		$E_TV_T\ T\ A_{u,l}$ [N]		
84×10^6		1.68×10^5		1.59×10^6		
TRC tensioned skin bending stiffness evolution deduced using the ACK approach						
B_{elas} [N.m^2]		$(B)_{multicrack}$ [N.m^2]		$B_{Textran}$[N.m^2]		
5488		Tangential stiffness depends on σ,ε		450		
Characteristic parameters of polyurethane shear stress vs angular strain law of behavior						
E_E(MPA)	Υ_E	τ_E (MPa)	Υ_F	τ_F (MPa)		
3.03	4.6×10^{-2}	0.18	0.28	0.36		

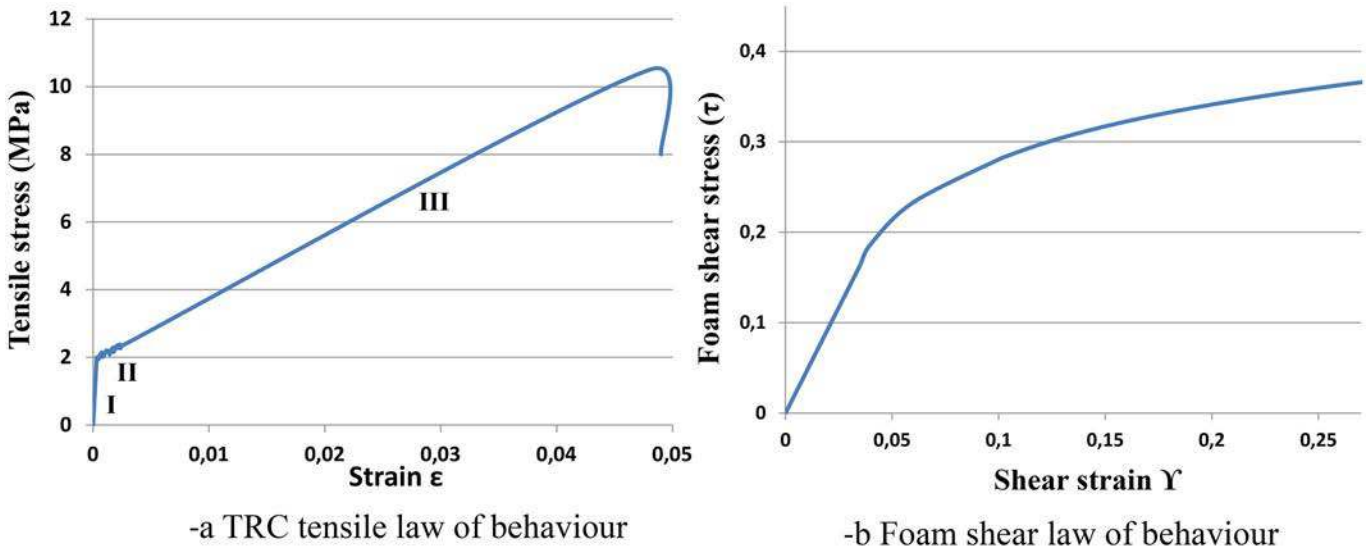

Figure 8. TRC and foam constitutive laws of behavior.

3.1.2.2. Local behavior in lower TRC facing. Due to the very thin layer of concrete cover (≈1mm, characteristic of TRC), the strain in the most tensioned textile fabric evaluated analytically by strain superposition of the two effects of M_s and M_l can be compared to the measurement of the LVDT sensor.

The strain in the most tensioned textile fabric ε_{max} of the lower TRC skin (due to the effects of the sandwich moment M_s and bending moment of TRC on its own axes due to M_l) predicted by the model at mid span is therefore compared with the strain measured by the LVDT sensor placed at mid span of the lower TRC skin and covering a measurement length of 200 mm in Figure 10 ($\varepsilon = \frac{\text{displacement measured by LVDT}}{\text{LVDT length}}$) .

The result predicted by the analytical model in agreement with the experimental measurement of tensile strain in the tensioned TRC skin (Figure 10), confirms that the initiation of the sandwich panel nonlinear behavior at an applied load of 2900 N is due to TRC multicracking leading to the textile transmission of load in the tensioned TRC facing (the crack pattern in the lower TRC skin at crack stabilization is shown Figure 10). Furthermore, the developed model is able to capture the evolution of the strain in the lower TRC skin textile fabric during multicracking and textile load transmission with a good precision (with a slight difference between the model and experimentation near failure due to the difficulty of the precise evaluation of the homogenized foam shear stiffness during foam hardening).

Figure 11 separates analytically (thanks to the developed model) the two contributions of the sandwich moment M_s and TRC lower skin bending moment around its own axis M_l on the evolution of strain in the most tensioned textile fabric ε_{max} of the lower TRC skin.

A-In the elastic phase [0-2900N]: The strain due to M_s and M_l increases linearly with the applied force. However the contribution of M_l on strain when the first crack occurs ($\varepsilon_{crack} = 2{,}17\times10^{-4}$) is much higher than M_s (see magnified Figure 11 in the first stage). In fact, the strain attributed to M_l is $\varepsilon_{M_l} = 1.85\times10^{-4}$ (≈85% of the strain at first crack) while the strain related to M_s is $\varepsilon_{M_s} = 3.2\times10^{-5}$ (≈15% of the strain at first crack). This can be explained by the significant bending stiffness of the lower TRC skin around its own axes in the elastic stage. In fact, for the faces and core to remain in contact during bending of the sandwich panel, the faces must bend to an infinite curvature due to foam shear strain. This is physically impossible. Instead, the skins bend locally around their own axes (see Figure 1) and the local bending moment of the skins (around their own axis) is proportional to the skin bending stiffness which explains the large contribution of M_l on strain when the first crack occurs in the lower TRC skin.

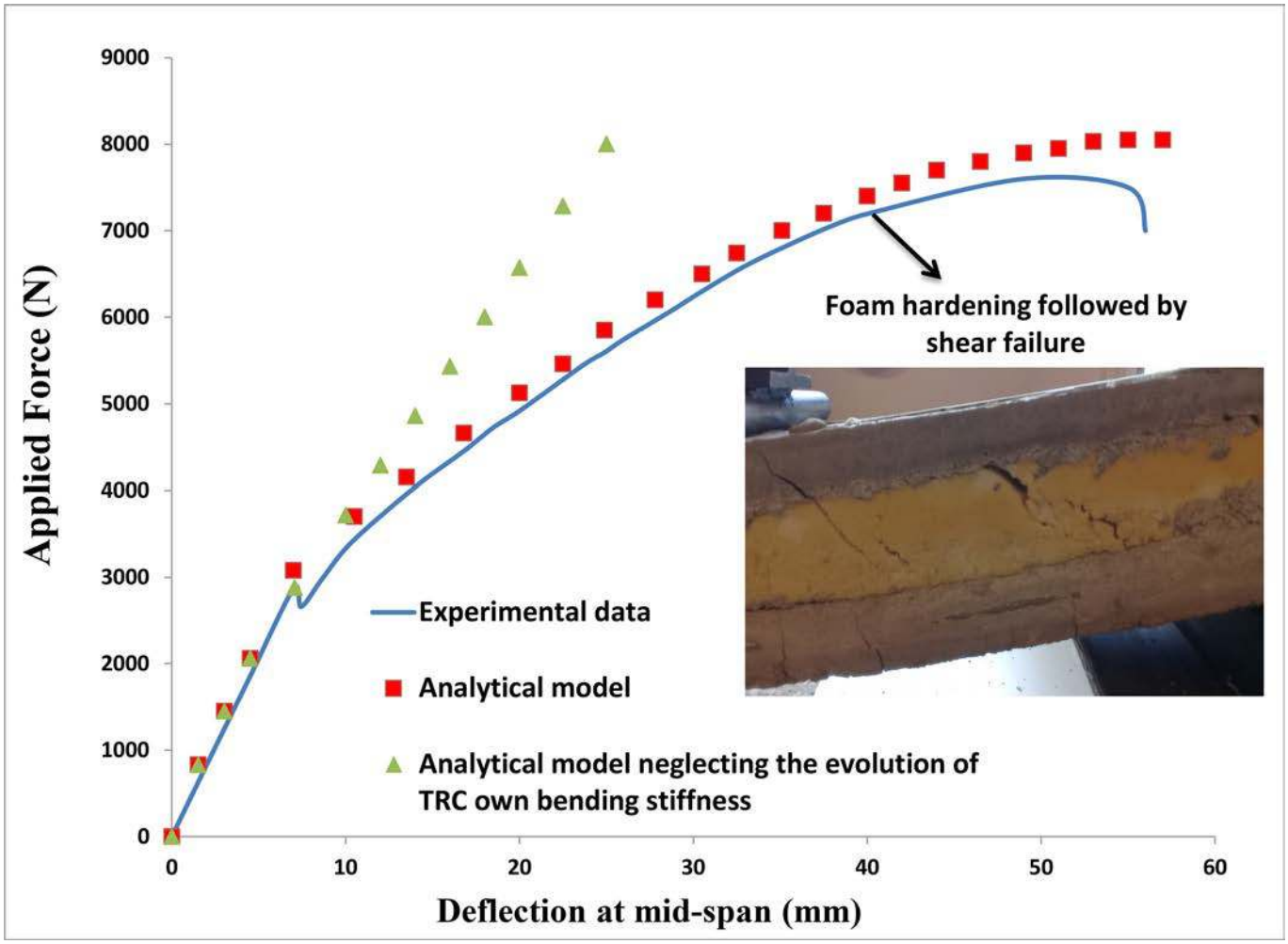

Figure 9. Comparison of analytical model and experimental data for the global behavior.

Analytically, this is reflected in the Stamm and Witte [15] solution for a sandwich beam under point load solicitation where the term α_l represents the effect of TRC bending stiffness and the term D represents the contribution of foam shear strain on the evolution of M_l (Eq. 29), see also Appendix.

$$M_s = P\ L\ \frac{1}{1+\alpha}\left[\underbrace{(1-\mu)\xi}_{B} - \underbrace{\frac{\sinh[\lambda(1-\mu)]}{\lambda\sinh\lambda}\sinh(\lambda\xi)}_{C}\right] \tag{28}$$

$$M_l = P\ L\frac{\alpha_l}{1+\alpha}\left[\underbrace{(1-\mu)\xi}_{B} + \underbrace{\frac{\sinh[\lambda(1-\mu)]}{\alpha\lambda\sinh\lambda}\sinh\lambda\xi}_{D}\right] \tag{29}$$

$$\alpha_l = \frac{B_l}{B_s},\quad \alpha = \frac{B_u + B_l}{B_s},\quad \beta = \frac{B_s}{AL^2}$$

$$\text{with } A = Gb_p\frac{c^2}{t_{core}},\quad \lambda = \sqrt{\frac{1+\alpha}{\alpha\beta}}$$

Remark: The term B in the Eqs. (28) and (29) reflects the expression of M_s and M_l considering the classic sandwich beam theory (neglecting foam shear strain), whereas the terms C and D reflect the contribution of foam shear strain on the evolution of M_s and M_l, respectively [when G (foam shear stiffness) tends to infinite, λ tends to infinite and the terms C and D tend to 0 (classic sandwich beam theory)]

B-In the multicracking phase [2900-3600N]: When multicracking occurs, a rapid increase of strain due to the two contributions of M_s and M_l is observed. This increase is attributed to the degradation of the axial and bending stiffnesses of the lower TRC skin. This phase ends when the strain due to the two contributions of M_s and M_l ($\varepsilon_{M_s}+\varepsilon_{M_l}$) reaches the strain at crack stabilization ($\varepsilon_{EMC} = 2.2\times10^{-3}$).

C-In the textile transmission phase [3600-7300N]: The quasi constant slope of the curves of (strain due to M_s versus applied force) and (strain due to M_l versus applied force) is attributed to the fact that the sandwich beam stiffness B_s (which dictates the evolution M_s) and lower TRC bending stiffness B_l (which dictates the evolution M_l) respectively tend to (are approximately):

$$B_s = \frac{(EA)_{texttrans} \times (EA)_u\ c^2}{(EA)_{textrans} + (EA)_u} \tag{30}$$

$$B_l = B_{textrans} \tag{31}$$

where $(EA)_{texttrans}$ and $B_{textrans}$ are the axial and bending stiffness of the lower TRC skin at textile transmission, respectively.

$(EA)_u$ is the axial stiffness of the upper TRC skin (which remains elastic).

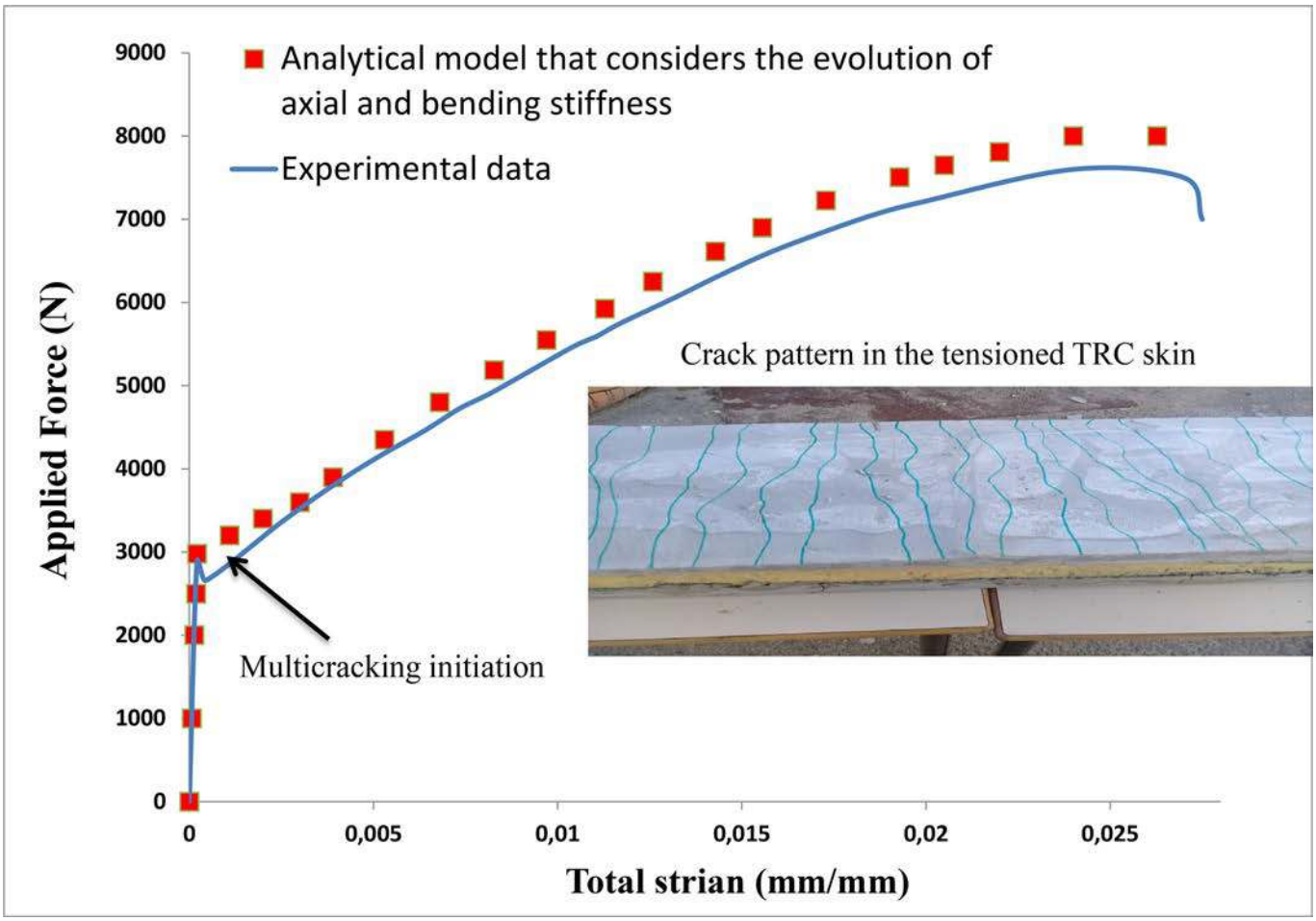

Figure 10. Comparison of Analytical model and experimental data for local behavior of TRC skin.

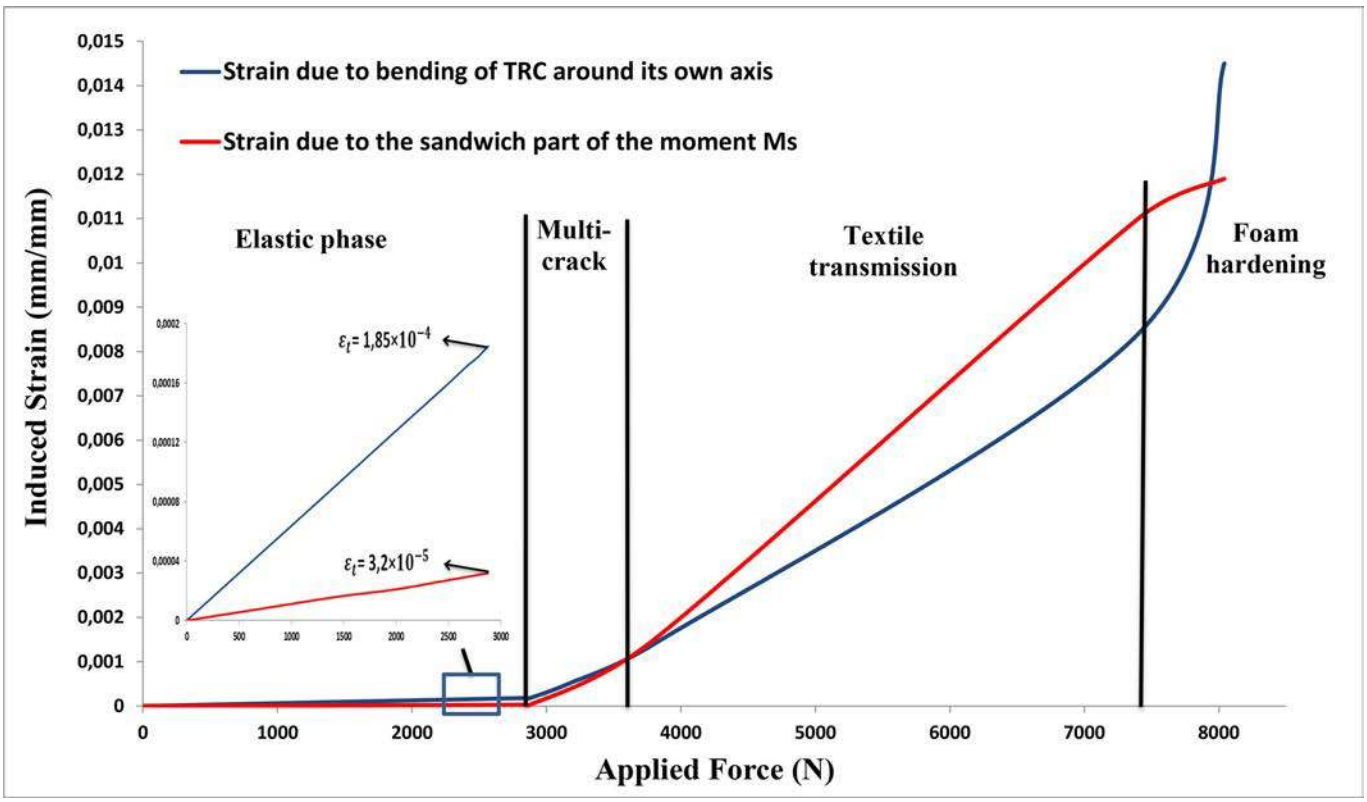

Figure 11. Contribution of M_s and M_l on the evolution of strain in the most tensioned textile fabric.

Table 2. State of strain in the lower TRC facing due to M_s and M_l.

(Force, deflection)	Normal strains due to bending of the tensioned TRC skin on their own axis (1)	Normal tensile strain due to the sandwich moment on TRC skin $N_s = \frac{M_s}{a}$ (2)	Maximum tensile strain in textile the fiber (1)+(2), ε_{max} $(\varepsilon_t + \varepsilon_{pt})$
(2900 N, 7,07 mm) End of the elastic phase	$\varepsilon_c = -1{,}85\times10^{-4}$ $\varepsilon_t = 1{,}85\times10^{-4}$ a= 14 mm b= 0 b_1= 0 b_2= 0	$\varepsilon_{pt} = 3{,}2\times10^{-5}$	$\varepsilon_{max} = 2{,}17\times10^{-4}$
(3600 N, 12,7 mm) End of the multicracking phase	$\varepsilon_c = -9{,}23\times10^{-4}$ $\varepsilon_t = 1{,}1\times10^{-3}$ a= 9,1 mm b= 1,2 mm b_1= 17,7 mm b_2= 0	$\varepsilon_{pt} = 1{,}1\times10^{-3}$	$\varepsilon_{max} = 2{,}2\times10^{-3}$
(7300 N, 42,1 mm) End of the textile transmission phase	$\varepsilon_c = -1{,}84\times10^{-3}$ $\varepsilon_t = 8{,}69\times10^{-3}$ a= 5 mm b= 0,6 mm b_1= 22,4 mm b_2= 13,5 mm	$\varepsilon_{pt} = 1{,}1\times10^{-2}$	$\varepsilon_{max} = 1{,}97\times10^{-2}$
(8000 N, 55 mm) Failure (Foam shear crushing)	$\varepsilon_c = -2{,}41\times10^{-3}$ $\varepsilon_t = 1{,}45\times10^{-2}$ a= 4 mm b= 0,3 mm b_1= 23,7 mm b_2= 18,2 mm	$\varepsilon_{pt} = 1{,}2\times10^{-2}$	$\varepsilon_{max} = 2{,}65\times10^{-2}$

At this moment, the strains dues to M_s and M_l are expressed according to Eq. (32) and (33), respectively

$$\varepsilon_{M_s} = \frac{\Delta M_s}{C\ E_T V_T\ T} + \varepsilon_{M_{s0}} \tag{32}$$

$$\varepsilon_{M_l} = \frac{\Delta M_l - b^2 \frac{\sigma_{MC}}{3} - \sigma_{MC} b_1 \left(\frac{b_1}{2} + b\right) + E_T V_T T \frac{b_2}{2}\left(h - a - \frac{b_2}{3}\right)\varepsilon_{EMC}}{E_C \frac{a^3}{3(h-a)} + E_T V_T\ T\ \frac{b_2}{2}\left(h - a - \frac{b_2}{3}\right)} + \varepsilon_{M_{l0}} \tag{33}$$

Equation (33) is derived from Eq. (24). The symbols a, b, b_1, b_2 refer to the distances used in the Section 2.3.1.2 (see Figure 3, these distances evolve during bending of TRC skin) to describe the distribution of stress along the TRC cross section due to bending around its own axis.

$\varepsilon_{M_{s0}}$ and $\varepsilon_{M_{l0}}$ are the strains due to M_s and M_l at the initiation of textile transmission phase, respectively.

ΔM_s and ΔM_l are the increments of M_s and M_l at the initiation of textile transmission phase, respectively.

- The higher slope of the curve of (strain due to M_s versus applied force) in comparison to the curve of (strain due to M_l versus applied force) in the textile transmission phase (unlike the elastic phase) can be explained by the continuous evolution of the neutral axis of the lower TRC skin during bending around its own axis [see Eq. (33), the increase of the distances b_1, b_2 with the decrease of the distance a (position of the neutral axis with respect to the compressed fiber due to bending of TRC around its own axis) when M_l increases during bending of TRC skin around its own axis explains the decease of the slope of the curve of (strain due to M_l versus applied force) in comparison to the curve (strain due to M_s versus applied force)].
- Despite the decrease of the contribution of M_l on the evolution of the strain in the most tensioned fabric in the textile transmission phase, it represents 44.1% of the total strain at an applied force of 7300 N (which corresponds to the beginning of the foam hardening phase)
- **In the foam hardening phase [7300N to failure]:** the much higher contribution of M_l in comparison to M_s on the evolution of the strain in the lower TRC skin can be explained by the continuous decrease of the foam shear stiffness G (due to foam hardening) and thus the continuous increase of foam shear strain. To remain in contact with the foam during its continuous shear deformation, the lower TRC skin must bend locally around its own axis. At this moment, the bending moment of the lower TRC skin around its own axis is proportional to TRC bending stiffness (lower skin has significant bending stiffness), which explains the significant increase of strain due to M_l (the quasi entire strain in the lower skin at the approach of shear failure is due to M_l because foam shear stiffness G approaches zero)

Analytically, this is reflected in the Stamm and Witte [15] solution for a sandwich beam under point load solicitation. As G approaches zero, λ tends to zero and the term D in the expression of M_l (see Eq. 29) approaches an asymptote equal to $\frac{\mu\xi}{\alpha}$ and M_l in turn approaches its maximum [simultaneously, the term C (see Eq. 28) approaches an asymptote equal to $\mu\xi$ and M_s approaches its minimum]

- The detailed state of strain in the lower TRC skin due to M_s and M_l at the end of each phase described above is resumed Table 2 (the symbols a, b, b_1, b_2 refer to the distances used in the Section 2.3.1.2 (Figure 3) to describe the distribution of stress along the TRC cross section due to bending around its own axis).

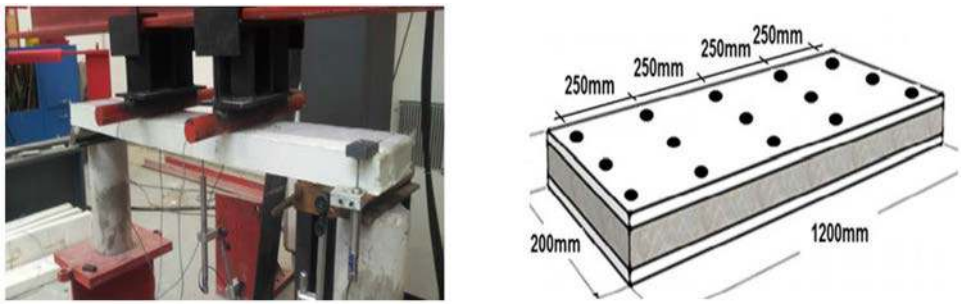

Figure 12. Four points bending test for TRC sandwich panels described in [6].

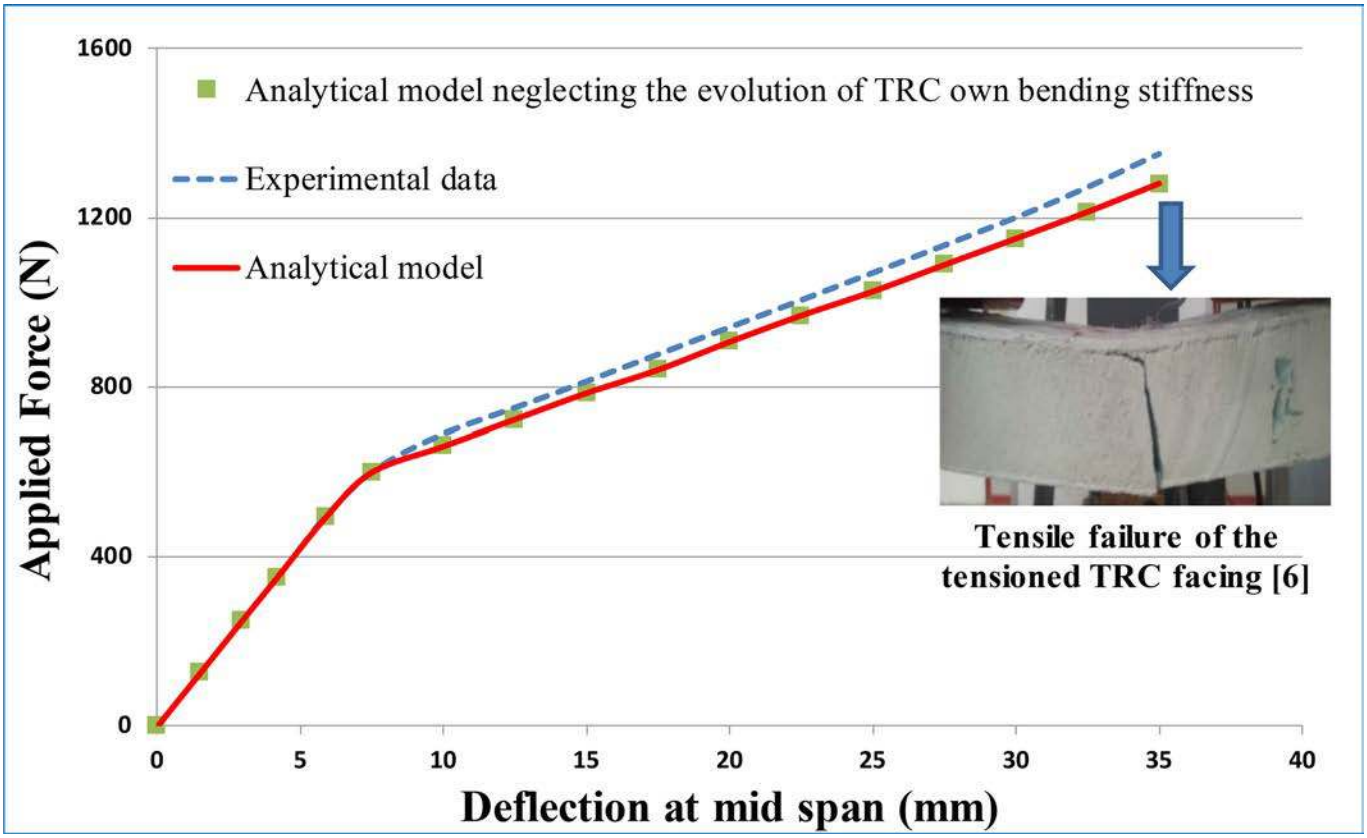

Figure 13. Analytical model vs Experimental data [6] (global panel behavior).

- It can be concluded from the above description of the evolution of strain in the most tensioned textile fabric during loading, that the accurate evaluation of the strain due to the contributions of M_s and M_l is necessary to achieve a precise evaluation of the sandwich panel homogenized axial and bending skin stiffness (according to Eqs. 25 and 26 which use $\varepsilon_{u,1}(x_i)_{j_{max}}$ as weighting factor) and thus an adequate load–deflection behavior. This explains the inaccurate evaluation of the sandwich panel behavior by the analytical model that only considers the evolution of TRC axial stiffness (Figure 9).

3.2. Validation of the analytical model on other TRC sandwich panels cases (panels with low TRC bending stiffness)

The objective of this part is to test the efficiency of the proposed analytical model on TRC sandwich panels tested in literature and for which the thickness of TRC skin is significantly lower compared to that of the foam core.

3.2.1. Model validation on the panel tested by Junes et al. [6]

The performance of the proposed analytical model has been also compared with the result of an experimental study conducted by Junes et al. [6] on a TRC sandwich panel.

The panel (1100 mm span × 56 mm thick × 200 wide) consists of two TRC skins (3-4 mm thick), and an insulation layer made of polyurethane PU 200(50 mm thick) shown Figure 12. The panel has been tested in four points bending with a panel span of 1100 mm (with a distance of 350 mm between the loading knives and the supports).

TRC facing consists of a fine-grained concrete reinforced with two layers of AR glass textile MAT [6].

Table 3. Analytical prediction of the State of strain in the lower TRC facing due to M_s and M_l [6].

(Force, deflection)	Normal strains due to bending of the tensioned TRC skin on their own axis (1)	Normal tensile strain due to the sandwich moment on TRC skin $N_s = \frac{M_s}{d}$ (2)	Maximum tensile strain in the textile fiber (1)+(2), ε_{max} $(\varepsilon_t + \varepsilon_{pt})$
(300 N, 3,56 mm) elastic phase	$\varepsilon_c = -1{,}03\times10^{-5}$ $\varepsilon_t = 1{,}03\times10^{-5}$ a= 2 mm b = 0 b_1=0 b_2=0	$\varepsilon_{pt} = 1{,}8\times10^{-4}$	$\varepsilon_{max} = 1{,}9\times10^{-4}$
(620 N, 7,6 mm) End of the elastic phase	$\varepsilon_c = -2{,}1\times10^{-5}$ $\varepsilon_t = 2{,}1\times10^{-5}$ a= 2 mm b= 0 b_1= 0 b_2= 0	$\varepsilon_{pt} = 3{,}72\times10^{-4}$	$\varepsilon_{max} = 3{,}74\times10^{-4}$
(900 N, 20 mm) Textile transmission phase	$\varepsilon_c = -1{,}2\times10^{-4}$ $\varepsilon_t = 2{,}4\times10^{-4}$ a= 1,3 mm b= 0,2 mm b_1= 2,5 mm b_2= 1,4 mm	$\varepsilon_{pt} = 5{,}36\times10^{-3}$	$\varepsilon_{max} = 5{,}6\times10^{-3}$
(1300 N, 35 mm) Textile tensile failure	$\varepsilon_c = -1{,}43\times10^{-4}$ $\varepsilon_t = 4{,}3\times10^{-4}$ a= 1 mm b= 0,1 mm b_1= 3,2 mm b_2= 2,1 mm	$\varepsilon_{pt} = 1{,}25\times10^{-2}$	$\varepsilon_{max} = 1{,}29\times10^{-2}$

The characteristic parameters of the TRC skins and foam laws of behavior under respectively direct tensile and pure shear solicitation can be found in [6].

The new analytical model for TRC sandwich panel and the experimental result are compared in terms of force transmitted vs deflection at mid span until failure; the two curves are plotted Figure 13. A third curve is also illustrated Figure 13 (**in small green squares**). It presents the analytical prediction of the sandwich panel behavior by considering the TRC skins stiffness on their own axis constant and equal to their elastic stiffness (neglecting the evolution of TRC skins bending stiffness and as consequence neglecting the induced strain attributed to bending of TRC skins on their own axis due to $M_{u,1}$) during the loading.

While it can be seen a good matching between the analytical model and the experimental data [6], the main conclusion that can be drawn is that the analytical model that neglects the evolution of TRC bending stiffness is also able to capture the global behavior of TRC sandwich panel (quasi identical result with the model that considers either the evolution of TRC axial or bending stiffness).This can be explained by the excessive low TRC skins bending stiffness [$B_{u,1} \approx 20.25\,\mathrm{N}m^2 \ll$ B (sandwich panel stiffness) $= 38395.51\,\mathrm{N}m^2$].

Table 3 presented below shows the contributions of the sandwich moment M_s and bending moment of the TRC skin on its own axis M_l on the evolution of the strain in the most tensioned textile fabric of the lower TRC skin at some applied loads (The results presented in Table 3 are extracted from the analytical model that considers either the evolution of TRC skin axial or bending stiffness)

From Table 3, it can be concluded that the contribution of M_l on the evolution of the strain in the lower TRC textile fabric can be neglected comparing to the contribution of M_s due to the above mentioned excessively low bending stiffness of TRC skin.

3.2.2. Model validation on the panel tested by Colombo et al. [7]

The performance of the proposed analytical model has been validated on the basis of the experimental four point bending test on a TRC sandwich panel realized by Colombo et al. [7].

The tested panel (920 mm span × 120 mm thick × 300 wide) consists of two TRC skins (10 mm thick) and an insulation layer made of expanded polystyrene EPS 250 (100 mm thick). The panel has been tested in four points bending with a panel span of 920 mm (with a distance of 306 mm between the loading knives and the supports). TRC and foam laws of behavior are described in [7].

The new analytical model for TRC sandwich panel (with and without consideration of the evolution of TRC bending stiffness) and the experimental result are compared in terms of force transmitted vs imposed stroke until failure; the two curves are plotted Figure 14.

A fourth curve is also presented Figure 14. It represents the prediction of the sandwich panel behavior by a numerical model developed by the authors of this paper in the commercial software ABAQUS. The details of the model are presented in [10]. It should be emphasized that a rigorous description of the foam and TRC skins behavior has been integrated in the numerical model developed in [10].

While it can be seen a good matching between the analytical model and the experimental data [7], the main conclusion that can be drawn is that the analytical model that neglects the evolution of TRC bending stiffness is able as well to capture the global behavior of TRC sandwich panel. However, a slight difference (7% at failure) exists between

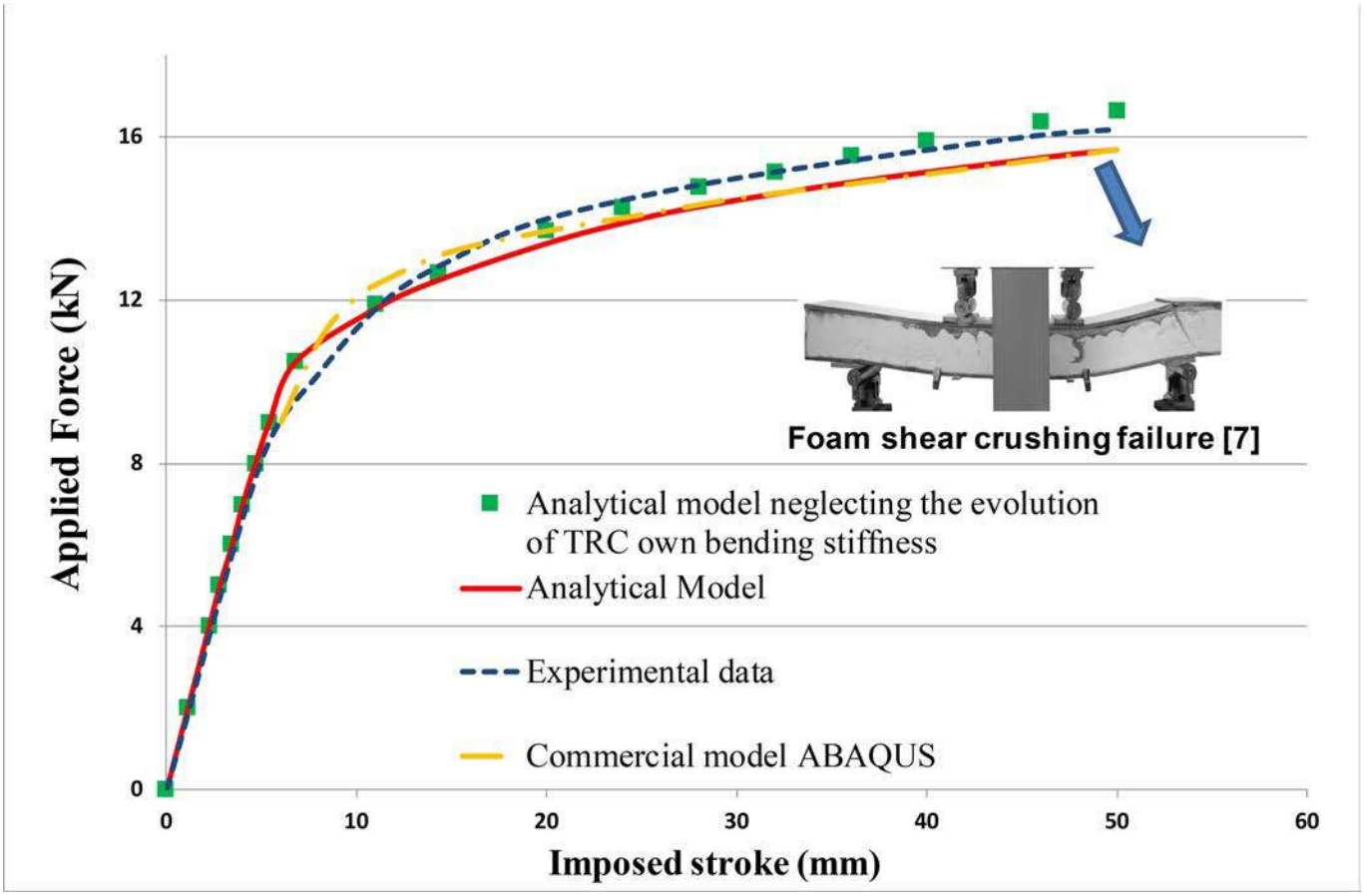

Figure 14. Analytical model vs numerical model vs Experimental data [7].

the analytical model that considers the two evolutions of TRC axial and bending stiffness and the model that neglects the evolution of TRC bending stiffness. This difference is due to foam hardening that occurs at 10.5 kN, which induces the continuous decrease of the foam shear stiffness G and thus the continuous increase of foam shear strain. To remain in contact with the foam during its continuous shear deformation, the lower TRC skin must bend locally around its own axis which induces an increase of the strain due to M_l and explains the slight difference between the analytical model that considers the two evolutions of TRC axial and bending stiffness and the one that neglects the evolution of TRC bending stiffness [in fact, the consideration of the evolution of axial and bending stiffness of TRC induces an increase of the total strain in the lower TRC skin and thus a decrease of the homogenized lower TRC skin stiffness and as a consequence a slight decrease of the sandwich panel stiffness in comparison to the model that neglects the evolution of TRC bending stiffness].

On the basis of the differents model validations and model optimization, some recommandations for modeling and design of TRC sandwich panels can be provided for the user:

A/For panels with significant TRC facing thickness ($h_{TRC} \geq$15mm, according to model optimization): the full version of the model (considering the two contributions of M_s and M_l) should be considered.

B/For panels with reduced to moderate TRC facing thickness and with high slendrness: the reduced version of the model considering only the contribution of M_s can be considered.

From Figure 14, it can also be seen that, there is a good matching between the analytical and numerical prediction. However, a slight difference exists between the two models at 10.5 KN (at the moment of foam hardening). This can be explained by the difference between the two models in the way of modeling foam nonlinear behavior. In fact, the crushable foam model [10] implemented in ABAQUS software was used for foam modeling in the numerical simulation, while a model based on the homogenized shear stiffness was used in the analytical model.

The two TRC sandwich panel models (analytical + numerical) detect an accurate mode of failure (due to foam crushing) at approximately 15 kN. However, it should be emphasized, that the analytical consumes much less time computing **(few seconds of time computing for the analytical model versus 30 min to 1 h according to the mesh for 3D numerical model simulation).** In fact, numerical models are time consuming especially when considering concrete multicracking and textile/concrete bond behavior as in the case of TRC facing for TRC sandwich panels.

4. Conclusion

The proposed analytical model is an extension and improvement of the work performed by [6, 12]. The model is an

alternative to commercial numerical models for either reproducing the global behavior of TRC sandwich panels under simply supported bending solicitation or detecting nonlinear behavior leading to failure of their components.

The proposed analytical model is based on the actualization of the state of normal strains in TRCs facings and shear strain in the foam core before reevaluating the panel homogenized stiffness and using the Stamm and Witte [15] differential equations solution.

The new TRC sandwich panel theoretical model considers possible significant bending stiffness of TRC skins on their own axes and uses the ACK approach to evaluate TRC axial and bending stiffness in the multicracking and textile transmission phases during sandwich panel bending. Furthermore, the model allows the consideration of foam hardening.

The model accurately evaluates the experimental load–deflection behavior of a TRC sandwich panel characterized by its significant skin bending stiffness. Furthermore, the model allows an estimation of the strain in the textile fabric attributed to the bending moment of TRC around its own axis M_l and the sandwich panel bending moment M_s.

The developed model could be presented as a tool to facilitate the integration of TRC in the building industry without considering excessive security factors. Moreover, the analytical method proposed could be presented as an indicator of load bearing capacity of TRC sandwich panels under simply supported bending solicitation in service and ultimate states.

Future research could possibly extend the application of this analytical model to random boundary conditions rather than its current application to only simply supported panels.

Acknowledgments

The authors thanks KAST company (Sonthofen, Germany) for providing the textile reinforcement used in the study.

Disclosure statement

All authors declare that they have no conflict of interest.

Funding

This study was funded by the Academic research community (ARC ENERGIES and SCUSI) of the Rhone-Alpes and Auvergne FRANCE region.

References

[1] K. Padmanabhan, Strength-based design optimization studies on rigid polyurethane foam core-glass and carbon-glass fabric face sheet/epoxy matrix sandwich composites, Mech. Adv. Mater. Struct., vol. 21, no. 3, pp. 191–196, 2014. DOI: 10.1080/15376494.2013.834093.

[2] X. Li, L. Wu, L. Ma, and X. Yan, Compression and shear response of carbon fiber composite sandwich panels with pyramidal truss cores after thermal exposure, Mech. Adv. Mater. Struct., vol. 26, no. 10, pp. 866–877, 2019. DOI: 10.1080/15376494.2018.1430269.

[3] Smitha Gopinath, V. Ramesh, A. Harishkumar Sheth, Ramachandra Murthy, and NageshR. Iyer, Pre-fabricated sandwich panels using cold-formed steel and textile reinforced concrete, Constr. Build. Mater., vol. 64, pp. 54–59, 2014. DOI: 10.1016/j.conbuildmat.2014.04.068.

[4] M. Saad, N. Lampros, and DionysiosA. Bournas, Textile-reinforced mortar (TRM) versus fibre-reinforced polymers (FRP) in flexural strengthening of RC beams, Constr. Build. Mater., vol. 151, pp. 279–291, 2017. DOI: 10.1016/j.conbuildmat.2017.05.023.

[5] A. Shams, M. Horstmann, and J. Hegge, Experimental investigations on Textile-Reinforced Concrete (TRC) sandwich sections, Compos. Struct., vol. 118, pp. 643–653, 2014. DOI: 10.1016/j.compstruct.2014.07.056.

[6] A. Junes and A. Si-Larbi, An experimental and theoretical study of sandwich panels with TRC facings: use of metallic connectors and TRC stiffeners, Eng. Struct., vol. 113, pp. 174–185, 2016. DOI: 10.1016/j.engstruct.2016.01.042.

[7] I. Colombo, M. Colombo, and M. Di Prisco, Bending behaviour of Textile Reinforced Concrete sandwich beams, Constr. Build. Mater., vol. 95, pp. 675–685, 2015. DOI: 10.1016/j.conbuildmat.2015.07.169.

[8] J. Vervloet, et al., Experimental investigation of the buckling behaviour of Textile Reinforced Cement sandwich panels with varying face thickness using Digital Image Correlation, Constr. Build. Mater., vol. 194, pp. 24–31, 2019. DOI: 10.1016/j.conbuildmat.2018.11.015.

[9] H. Cuyper and J. Wastiels, Analysis and verification of the performance of sandwich panels with Textile reinforced concrete faces, J. Sandwich Struct. Mater., vol. 13, no. 5, pp. 589–603, 2011. DOI: 10.1177/1099636211408665.

[10] Z.I. Djamai, M. Bahrar, F. Salvatore, A. Si Larbi, and M. El-Mankibi, Textile reinforced concrete multiscale modeling: Application to TRC sandwich panels, Finite Element Des. Anal., vol. 135, pp. 22–35, 2017. DOI: 10.1016/j.finel.2017.07.003.

[11] N.W. Portal, M. Flansbjer, K. Zandi, L. Wlasak, and K. Malaga, Bending behaviour of novel Textile Reinforced Concrete-foamed concrete (TRC-FC) sandwich elements, Compos. Struct., vol. 177, pp. 104–118, 2017. DOI: 10.1016/j.compstruct.2017.06.051.

[12] A. Shams, J. Hegger, and M. Horstmann, An analytical model for sandwich panels made of textile reinforced concrete, Constr. Build. Mater., vol. 64, pp. 451–459, 2014. DOI: 10.1016/j.conbuildmat.2014.04.025.

[13] J. Blom, H. Cuypers, P. Van Iterbeek, and J. Wastiels, Determination of material parameters of a textile reinforced composite using an inverse method, ECCCM 13 Conference, Stockholm, 2008.

[14] H.G. Allen, Analysis and Design of Structural Sandwich Panels, Pergamon Press, Oxford, 1993.

[15] K. Stamm and H. Witte, Sandwichkonstruktionen-Berechung, Fertigung, Ausfuhrung, Springer Verlag, New York, 1974.

[16] J. Hegger, N. Will, O. Brckermann, and S. Voss, Load bearing behaviour and simulation of textile reinforced concrete, Mater. Struct., vol. 39, no. 8, pp. 765–776, 2006. DOI: 10.1617/s11527-005-9039-y.

[17] G. Promis, A. Gabor, G. Maddaluno, and P. Hamelin, Analytical modeling of the bending behavior of textile reinforced mineral matrix composite beams, Compos. Struct., vol. 92, no. 10, pp. 2565–2572, 2010. DOI: 10.1016/j.compstruct.2010.02.003.

[18] L. Gibson and M. Ashby, Cellular Solids: Structure and Properties, Cambridge university press, Cambridge, 1997.

[19] RILEM Technical Committee. Recommendation 232-TDT: test methods and design of TRC, Mater. Struct., vol. 49, 4923–4949, 2016.

Appendix

Stamm and Witte [15] offer a system solution for a simply supported beam subjected to uniformly distributed load and point load. The solution for point load solicitation at any position x is given as follows:

Index 1 is assigned for $0 \leq \xi \leq \mu$ and 2 for $\mu \leq \xi \leq 1$ where $\mu = \frac{e}{L}$ (e is the longitudinal coordinate of the load application on the panel span L) and $\xi = \frac{x}{L}$,

$$w_1 = \frac{PL^3}{B}\left[\frac{1}{6}(1-\mu)\xi\ \left(2\mu - \mu^2 - \xi^2\right) + \frac{1}{\alpha\lambda^2}(1-\mu)\xi - \frac{1}{\alpha\lambda^3}\ \frac{\sinh[\lambda(1-\mu)]}{\sinh\lambda}\ \sinh(\lambda\xi)\right]$$

$$w_2 = \frac{PL^3}{B}\left[\frac{1}{6}(1-\xi)\ \mu\ \left(2\xi - \mu^2 - \xi^2\right) + \frac{1}{\alpha\lambda^2}(1-\xi)\ \mu - \frac{1}{\alpha\lambda^3}\ \frac{\sinh(\lambda\mu)}{\sinh\lambda}\ \sinh[\lambda(1-\xi)]\right]$$

$$\Upsilon_1 = \frac{PL^2}{B}\ \beta\ \left[(1-\mu) - \frac{\sinh[\lambda(1-\mu)]}{\sinh\lambda}\ \cosh(\lambda\xi)\right]$$

$$\Upsilon_2 = \frac{PL^2}{B}\ \beta\left[-\mu + \frac{\sinh(\lambda\mu)}{\sinh\lambda}\ \cosh[\lambda(1-\xi)]\right]$$

$$M_{s1} = P\ L\frac{1}{1+\alpha}\left[(1-\mu)\ \xi - \frac{\sinh[\lambda(1-\mu)]}{\lambda\sinh\lambda}\ \sinh(\lambda\xi)\right]$$

$$M_{s2} = P\ L\frac{1}{1+\alpha}\left[(1-\xi)\ \mu - \frac{\sinh(\lambda\mu)}{\lambda\sinh\lambda}\ \sinh[\lambda(1-\xi)]\right]$$

$$M_{u,l\ 1} = P\ L\frac{\alpha_{u,l}}{1+\alpha}\left[(1-\mu)\xi + \frac{\sinh[\lambda(1-\mu)]}{\alpha\lambda\sinh\lambda}\ \sinh\lambda\xi\right]$$

$$M_{u,l\ 2} = P\ L\frac{\alpha_{u,l}}{1+\alpha}\left[(1-\xi)\mu + \frac{\sinh(\lambda\mu)}{\alpha\lambda\sinh\lambda}\ \sinh[\lambda(1-\xi)]\right]$$

$$Q_{s1} = P\ \frac{1}{1+\alpha}\left[(1-\mu) - \frac{\sinh[\lambda(1-\mu)]}{\sinh\lambda}\ \cosh(\lambda\xi)\right]$$

$$Q_{s2} = P\ \frac{1}{1+\alpha}\left[-\mu + \frac{\sinh\lambda\mu}{\sinh\lambda}\ \cosh[\lambda(1-\xi)]\right]$$

$$\alpha_{u,l} = \frac{B_{u,l}}{B_s},\ \alpha = \frac{B_u + B_l}{B_s},\ \beta = \frac{B_s}{AL^2},\ \lambda = \sqrt{\frac{1+\alpha}{\alpha\beta}}$$